Title
Dark Matter Thermonuclear Supernova Ignition

Authors
Steigerwald, Heinrich
Profumo, Stefano
Rodrigues, Davi
et al.

Publication Date
2019-12-27

Peer reviewed

MNRAS 000, 1–21 (2019) Preprint 1 January 2020 Compiled using MNRAS LATEX style file v3.0

Dark Matter Thermonuclear Supernova Ignition

Heinrich Steigerwald,[1★] Stefano Profumo,[2] Davi Rodrigues,[1] Valerio Marra[1]
[1] *Center for Astrophysics and Cosmology (Cosmo-ufes) & Department of Physics, Federal University of Espírito Santo, Vitória, ES, Brazil*
[2] *Department of Physics and Santa Cruz Institute for Particle Physics, 1156 High St, University of California, Santa Cruz, CA 95064, USA*

Accepted XXX. Received YYY; in original form ZZZ

ABSTRACT

We investigate local environmental effects from dark matter (DM) on thermonuclear supernovae (SNe Ia) using publicly available archival data of 224 low-redshift events, in an attempt to shed light on the SN Ia progenitor systems. SNe Ia are explosions of carbon-oxygen (CO) white dwarfs (WDs) that have recently been shown to explode at sub-Chandrasekhar masses; the ignition mechanism remains, however, unknown. Recently, it has been shown that both weakly interacting massive particles (WIMPs) and macroscopic DM candidates such as primordial black holes (PBHs) are capable of triggering the ignition. Here, we present a method to estimate the DM density and velocity dispersion in the vicinity of SN Ia events and nearby WDs; we argue that (i) WIMP ignition is highly unlikely, and that (ii) DM in the form of PBHs distributed according to a (quasi-) log-normal mass distribution with peak $\log_{10}(m_0/1\,\mathrm{g}) = 24.9\pm0.9$ and width $\sigma = 3.3 \pm 1.0$ is consistent with SN Ia data, the nearby population of WDs and roughly consistent with other constraints from the literature.

Key words: dark matter – supernovae: general – white dwarfs

1 INTRODUCTION

It is difficult to overstate the importance of type Ia supernovae (SNe Ia) for cosmology, including their role in the discovery of the accelerated expansion of the universe (Riess et al. 1998; Perlmutter et al. 1999), thanks to the tight empirical correlation (Phillips 1993) between intrinsic peak luminosities and post-peak decline rates over 15 days. The underlying physics of SNe Ia is rather well understood as the explosion of degenerate carbon-oxygen (CO) white dwarf (WD) stars (Hoyle & Fowler 1960; Colgate & McKee 1969), where the absolute B-band peak luminosity stems from the amount of radioactive ^{56}Ni produced during the explosion (Stritzinger et al. 2006), and the post-peak decline rate $\Delta m_{15}(B)$ relates to the total ejected mass during the explosion (Scalzo et al. 2014), which, for total disruptions, is equal to the progenitor white dwarf mass, $M_{\rm wd}$.

The apparent standard candle nature of 'normal' SNe Ia (Branch et al. 1993) led to the popular belief that the explosion is triggered through self-ignition upon reaching the classical Chandrasekhar (1931) limit of 1.4 solar masses ($\mathrm{M}_\odot$) when the core reaches sufficiently high densities to ignite carbon runaway fusion spontaneously (Nelemans et al. 2001). Yet, newly born pure CO WDs are formed in the mass range from $0.6\,\mathrm{M}_\odot$ to $1.0\,\mathrm{M}_\odot$ (de Vaucouleurs & Corwin 1985). Heavier WDs contain an oxygen-neon-magnesium core and lighter ones present a helium surface layer (Dan et al. 2012). Therefore, it is usually assumed that SNe Ia happen in close double systems, where the Chandrasekhar mass is reached either through Roche lobe overflow from a non-degenerate binary companion star (Whelan & Iben 1973), or through the merger of double WDs (Iben & Tutukov 1984; Webbink 1984) and the subsequent accretion of the tidally disrupted secondary. These progenitor channels are known as the single degenerate scenario (SDS) and the double degenerate scenario (DDS).

It has been shown that the SDS can not account for more than 5 per cent of all SNe Ia due to the lack of supersoft X-ray emission in elliptical galaxies (Gilfanov & Bogdán 2010) and He II recombination lines (Woods & Gilfanov 2013). Moreover, the observation of sub-Chandrasekhar explosions (Scalzo et al. 2014) can not be explained in this scenario. Finally, the general absence of hydrogen in SN Ia spectra (Leonard 2007; Chomiuk et al. 2016) also disfavors this scenario to produce 'normal' SNe Ia. However, it could be the origin of some rare events with interaction of circumstellar medium (Ia-CSM subtype) playing an important role.

The DDS successfully explains the delay time distribution (Mennekens et al. 2010) and the overall rate (van Kerkwijk et al. 2010b). Furthermore, under the combined assumptions of a continuous mass spectrum (Scalzo et al. 2014) and pure CO detonations (supersonic fusion), the correct mix of iron and intermediate mass elements of 'normal' SNe Ia is successfully explained (Sim et al. 2010), as well

★ E-mail: heinrich@steigerwald.name

as over-luminous (91T-like) and under-luminous (91bg-like) sub-types at the far ends of Philips relation (Graham et al. 2018). Still, as we will argue in the following, the ignition mechanism remains unexplained.

First, numerical simulations of CO WD mergers show no sign of an explosion (Loren-Aguilar et al. 2009; Pakmor et al. 2010), unless in the presence of helium (Dan et al. 2012) via double-detonations (Woosley & Weaver 1986), or for total masses $> 1.8\,M_\odot$. Yet, helium detonations produce colors and spectra in contradiction with observations (Kromer et al. 2010; Sim et al. 2010; Howell 2011) and WD mergers with $> 1.8\,M_\odot$ are too rare and do not produce the observed decline rate (Pakmor et al. 2010). Only frontal WD collisions (Benz et al. 1989) lead to detonations (Rosswog et al. 2009), but even with Kozai-resonances in triple-systems (Thompson 2011), the rate can't account for all events (Katz & Dong 2012), even though they might be the origin of under-luminous Ia-91bg events (Vallely et al. 2019).

Second, the ignition is unlikely to occur during the post-merger accretion phase: As inferred from early light curves (Olling et al. 2015; Sasaki et al. 2018) and SN Ia remnants (Badenes et al. 2007), the circum-stellar medium surrounding the WD at the moment of the explosion is rather clean and empty. Also, the recently and first ever observed pure CO WD merger remnant 'WS35' did not explode during 16 thousand years of post-merger evolution (Gvaramadze et al. 2019).

Third, the ignition is still matter of controversy to occur at the end of the post-merger accretion phase. Due to conservation of angular momentum, the merger remnant is initially in rapid differential rotation which lowers the core density. According to Shapiro & Teukolsky (1986) merger remnants up to $2.5\,M_\odot$ are initially stabilized by rotation. The timescale of angular momentum loss is uncertain. According to Tornambé & Piersanti (2013), it requires at least several million years, but Schwab et al. (2016) argue that differential rotation turns on magnetic fields and viscous forces that slow down the rotation in 20 thousand years. According to Loren-Aguilar et al. (2009), compressional heating of the core could trigger the ignition, but it has also been argued that viscous heating increases the peak temperature only by a factor of two, while two orders of magnitude are necessary (Timmes & Woosley 1992). Therefore, the ignition is uncertain, especially for sub-Chandrasekhar mass WDs (Niemeyer & Woosley 1997; Sim et al. 2010).

Forth and last, but not least, fast decliners ($\Delta m_{15}(B) > 1.4$) or low mass explosions ($< 1.0\,M_\odot$) are difficult to explain by the merger of a WD binary. In addition to the absence of helium SN Ia spectra, the production time of these low mass WDs ultra-passes the age of the universe. If these events originate from lone CO WDs, then the ignition mechanism must be explained. Most intriguing, these events happen more often in older stellar environments (Gonzalez-Gaitan et al. 2011; Childress et al. 2014a) and more massive galaxies (Childress et al. 2014b), and, as we will show, they happen in dark matter denser environments.

Based on the above, we argue here that the ignition might be triggered by an external mechanism. One possibility is that the mechanism involves dark matter (DM). DM accretion onto stellar objects can lead to important effects, including for example fueling entire stages of stellar evolution ("*dark stars*", see e.g. Hall & Gondolo 2006), or destroying neutron stars by seeding rapidly-accreting black holes inside them (McDermott et al. 2012). The objective of this article is to show, with theoretical arguments and observational hints, that certain forms of DM possess the characteristics to trigger the ignition of SNe Ia.

Several dark matter thermonuclear supernova ignition models have been proposed recently: Graham et al. (2015) have shown that primordial black holes (PBH) heavier than 10^{19} g can trigger the ignition. Bramante (2015) has shown that weakly interacting massive particles (WIMPs) with mass 10^7 GeV and nuclear cross section $3 \times 10^{-42}\,\mathrm{cm}^2$ reproduce the age-mass relation of SN Ia events. Other studies include DM collapse (Leung et al. 2015; Graham et al. 2018) and BH evaporation (Acevedo & Bramante 2019; Janish et al. 2019). These studies assume a homogeneous DM distribution. However, the actual DM density in galaxies varies over several orders of magnitude (Navarro et al. 1996).

Here, we present a method to estimate the DM density ρ_χ and velocity dispersion v_χ in the vicinity of SNe Ia. To our knowledge, this has never been done before. The method is applied to archival SN Ia data, and a statistical analysis is performed. The best-fit DM ignition models are used to predict the ignition time of nearby WDs and the viability of each model is discussed.

The paper is organized as follows: in Section 2.1 we restate SN Ia ignition conditions; in Section 2.2 we review theoretical possibilities that lead to DM SN Ia ignition; in Section 2.3 we present a method to measure DM parameters in the vicinity of SNe Ia; in Section 2.4 we present the SN Ia data analysis; in Section 2.5 we review the progenitor channel assumptions; and in Section 2.6 we present a nearby WD coherence test. Results and discussion follow in sections 3 and 4 and we conclude in section 5.

Throughout this paper we index dark matter quantities by a 'χ', nuclear quantities by an 'n', white dwarf or supernova quantities by 'wd' and galactic quantities by a 'g'.

2 MODELS AND METHODS

2.1 Ignition conditions

According to the work of Timmes & Woosley (1992), for degenerate WD material with density $10^7 - 10^9\,\mathrm{g\,cm^{-3}}$, carbon runaway fusion is triggered if a small region of radius R_i exceeds the ignition temperature T_i such that it encloses $10^{-5} - 10^{15}$ g of WD matter and satisfying

$$R_\mathrm{i} \geq 1.5\,\mu\mathrm{m} \left(\frac{\rho_\mathrm{wd}}{10^8\,\mathrm{g\,cm^{-3}}}\right)^{-1/6} \left(\frac{T_\mathrm{i}}{4.3 \times 10^9\,\mathrm{K}}\right)^{-70/9} \quad (1)$$

As a second condition, the heat flow into the region must exceed the heat flow out of the region (Kippenhahn & Weigert 1990). At higher densities, heat diffusion is dominated by relativistic electron conduction and the opacity scales with density as $\propto \rho_\mathrm{wd}^{-2}$. At lower densities, heat diffusion is dominated by photons and the opacity scales with density as $\propto \rho_\mathrm{wd}$. Therefore, the heat equation implies

$$R_\mathrm{i} \geq 1.5\,\mu\mathrm{m} \left(\frac{\rho_\mathrm{wd}}{10^8\,\mathrm{g\,cm^{-3}}}\right)^{\zeta} \left(\frac{T_\mathrm{i}}{4.3 \times 10^9\,\mathrm{K}}\right)^{3/2} \quad (2)$$

where $\zeta = -1/2$ for $\rho_\mathrm{wd} > 10^8\,\mathrm{g\,cm^{-3}}$ and $\zeta = -2$ for $\rho_\mathrm{wd} < 10^8\,\mathrm{g\,cm^{-3}}$.

According to Seitenzahl et al. (2009), the geometry of the initial hot spot is arbitrary. However, in order for a detonation (supersonic fusion) front to form, the temperature profile of the initial hot spot must be steep, as has been shown by their numerical simulations. Since sub-Chandrasekhar explosions only reproduce observed SNe Ia under the assumption of detonations (Sim et al. 2010), we require, as a third condition, a steep temperature profile of the initial hot spot.

2.2 Dark Matter ignition channels

The mean encounter cross-section between DM particles and WDs is

$$\sigma_{\chi \rm wd} = \pi R_{\rm wd}^2 \left[1 + \left(\frac{v_{\rm e}}{v_\chi} \right)^2 \right], \quad (3)$$

where $R_{\rm wd}$ is the radius of the WD, v_χ is the velocity dispersion of DM particles in the halo at the position of the WD but outside its potential well, and the escape velocity at the surface of the WD is

$$v_{\rm e} = \left(\frac{2GM_{\rm wd}}{R_{\rm wd}} \right)^{1/2} \approx 6 \times 10^3 \, {\rm km\,s^{-1}} \left(\frac{M_{\rm wd}}{\rm M_\odot} \right)^{2/3}. \quad (4)$$

In equation (3), the term in brackets accounts for gravitational focussing (Lissauer 1993). Taking into account the number density $n_\chi = \rho_\chi / m_\chi$, where m_χ is the DM particle mass, encounters between DM particles and WDs occur at a rate

$$\Gamma_{\chi \rm wd} = \sigma_{\chi \rm wd} \, n_\chi \, v_\chi \approx \frac{2\pi G M_{\rm wd} R_{\rm wd} \rho_\chi}{m_\chi v_\chi}. \quad (5)$$

Note that the encounter rate of equation (5) is proportional to the DM density ρ_χ and inversely proportional to the velocity dispersion v_χ. The subsequent physics of the trigger mechanism depends on the DM mass m_χ and, potentially, on a non-gravitational interaction cross-section $\sigma_{{\rm n}\chi}$ between WD nuclei and DM particles. In Section 2.2.1, based on the ideas of Graham et al. (2015), we present the ignition by the passage a single macroscopic DM candidate or PBH through a WD, that we call the 'bullet mechanism'. In Section 2.2.2, based on the derivation of Bramante (2015), we present the ignition by a continuous accumulation of WIMPs in a WD, that we call the 'poison mechanism'.

2.2.1 Bullet mechanism

Primordial black holes (PBH) are a promising form of DM since they can potentially explain micro-lensing events, gravitational wave sources and the seeds of supermassive black holes in large galaxies. When a PBH of mass $m_\chi \sim 10^{24}$ g encounters a WD, it engulfs a negligible amount of WD nuclei on its passage and goes right through it like a bullet. Its strong gravitational attraction heats WD material in the vicinity of its trajectory. At relevant densities $\rho_{\rm wd} < 10^9 \, {\rm g\,cm^{-3}}$, the PBH's velocity inside the WD $v_\chi + v_{\rm e} \approx v_{\rm e}$ is larger than the sound speed (Timmes & Woosley 1992). Therefore, the resulting heating can be calculated in the sudden approximation.

Following the derivation of (Binney & Tremaine 1987, pp.33-36), the passage of a PBH accelerates WD nuclei in a cylindrical region of radius $R_{\rm i}$ to the mean-square velocity change

$$\langle \Delta v_{\rm n}^2 \rangle = 2 v_{\rm e}^2 \left(\frac{R_{\rm a}}{R_{\rm i}} \right)^2 \ln \left(\frac{R_{\rm i}}{R_{\rm a}} \right), \quad (6)$$

where $R_{\rm a} = 2 G m_\chi v_{\rm e}^{-2}$ is the accretion radius of the PBH and we have assumed that particles closer to the trajectory than the $R_{\rm a}$ get eaten by it (Bondi & Hoyle 1944) and are irrelevant for ignition heating. The mean-square velocity change of equation (6) must satisfy

$$\langle \Delta v_n^2 \rangle \geq \frac{3 k_{\rm B}}{m_{\rm n}} (T_{\rm i} - T_{\rm wd}), \quad (7)$$

where $T_{\rm i}$ is the ignition temperature (see Sec. 2.1), $T_{\rm wd}$ is the temperature of the WD and $m_n \approx 14$ GeV is the mean mass of CO nuclei.

The velocities $\boldsymbol{v}_{\rm n}$ acquired by nuclei are roughly perpendicular to the PBH trajectory and directed towards it with amplitudes inversely proportional to the impact parameter, thus creating a hot cylindrical region with a steep temperature profile and fulfilling the additional detonation condition required in Sec. 2.1. The minimum mass $m_\chi^{\rm min}$ we find is comparable to that found by Graham et al. (2015). We note that $m_\chi^{\rm min}$ is about one order of magnitude higher if Kelvin-Helmholtz instabilities occur (Montero-Camacho et al. 2019).

PBHs can be created during inflation as collapsed over-densities. A natural choice for their masses is an extended mass distribution, since the initial spectrum of over-densities is already extended. The phenomenon of critical collapse spreads the spectrum further out (Niemeyer & Jedamzik 1999). As pointed out by Green (2016), the final mass distribution of most inflationary models can be fitted by a (quasi-) log-normal distribution

$$\frac{{\rm d}n}{{\rm d}m_\chi} = N \exp \left[- \frac{\ln^2 (m_\chi / m_0)}{2\sigma^2} \right], \quad (8)$$

where m_0 and σ are peak and width of the distribution and N is a normalization constant. The difference of equation (8) and an (exact) log-normal distribution is a factor $1/m_\chi$. Finally, we define the mean time delay to ignition

$$\langle t_{\rm i} \rangle = \epsilon_{\rm sn} \left[\int_{m_\chi} \frac{{\rm d}n}{{\rm d}m_\chi} \Gamma_{\chi \rm wd}(m_\chi) \, \theta(m_\chi - m_\chi^{\rm min}) \, {\rm d}m_\chi \right]^{-1}, \quad (9)$$

where $\theta(x)$ is the Heaviside function, $m_\chi^{\rm min}$ is the minimal PBH mass obtained from equations (1), (2), (6) and (7), $\Gamma_{\chi \rm wd}(m_\chi)$ is the transit rate given by equation (5) and $\epsilon_{\rm sn}$ is the WD to SN conversion efficiency which is about one per cent (Pritchet et al. 2008). Note that equation (9) depends on $M_{\rm wd}$, ρ_χ, v_χ, m_0, σ and only weakly on $T_{\rm wd}$. It can be verified easily from equation (9) that, for example, lighter WDs explode later or only in DM denser environments. In particular, fast decliners or low mass explosions are excluded in regions of low DM density due to the finite age of the universe (see Fig. 1a).

2.2.2 Poison mechanism

This mechanism requires a small but non-zero interaction cross-section $\sigma_{\chi \rm n}$ between WIMPs and nuclei and possibly between WIMPs $\sigma_{\chi\chi}$, mediated by a non-gravitational force. The mechanism acts through capture of asymmetric (non

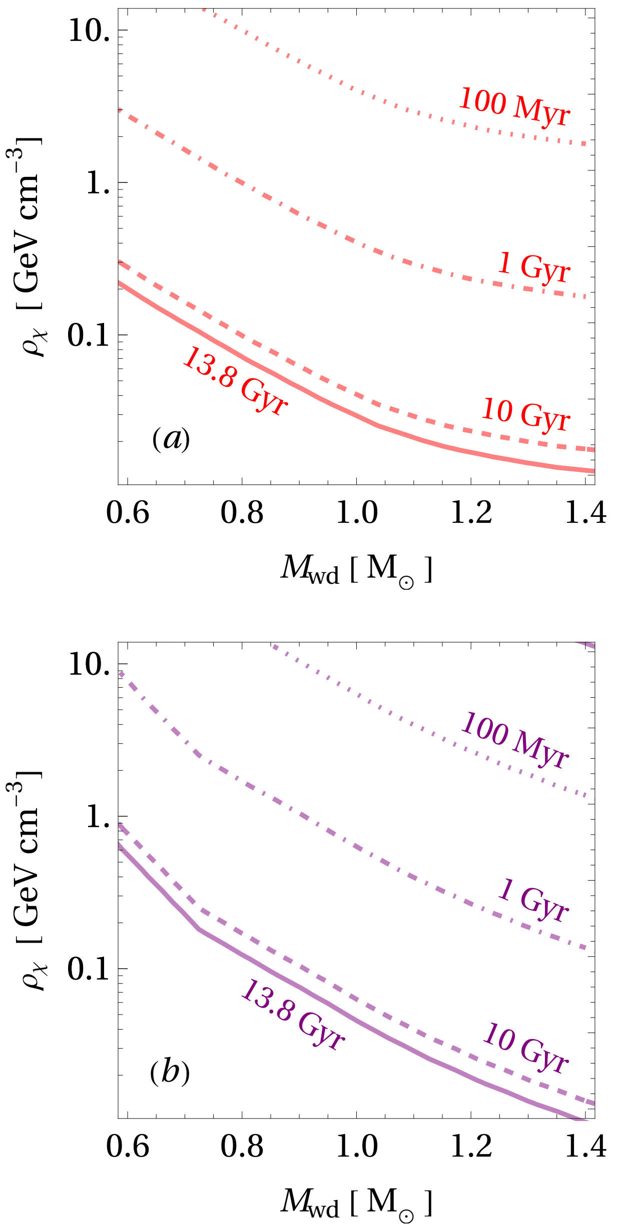

Figure 1. (a) mean ignition time $\langle t_{\rm i}\rangle$ for a (quasi-) log-normal distribution of PBHs with peak $m_0 = 10^{24}$g and width $\sigma = 3$, as a function of WD mass and DM density. (b) ignition time $t_{\rm i}$ for asymmetric WIMPs with mass $m_\chi = 10^8$ GeV and nuclear cross-section $\sigma_{n\chi} = 10^{-38}\,{\rm cm}^2$, as a function of WD mass and DM density. In both figures, we assume $v_\chi = 200\,{\rm km\,s}^{-1}$ and $T_{\rm wd} = 10^7$ K.

self-annihilating) WIMPs inside the WD potential well that will thermalise over time and eventually collapse shedding localized gravitational energy that triggers the ignition (Bramante 2015).

The capture of a particle by the WD is achieved if a diffusion with a WD nucleus induces an energy loss larger than $m_\chi\, v_\chi^2/2$. Assuming that DM particles are in thermodynamic equilibrium, the capture cross-section for WIMPs by a WD is (Gould 1987)

$$\Gamma_{\rm cap} = \sqrt{24\pi}\, G\, \frac{M_{\rm wd}\, R_{\rm wd}\, \rho_\chi}{m_\chi v_\chi}\, {\rm Min}\left(1, \frac{\sigma_{n\chi}}{\sigma_{\rm sat}}\right)\left[1 - \frac{1-e^{-B^2}}{B^2}\right], \quad (10)$$

where $B^2 = 6\, m_\chi v_{\rm e}^2/(m_\chi - m_{\rm n})^2\, v_\chi^2$, $m_{\rm n} \approx 14\,$GeV is the nuclear mass and $\sigma_{\rm sat} = \pi R_{\rm wd}^2/N_{\rm n}$ is the saturation cross-section where $N_{\rm n} = M_{\rm wd}/m_{\rm n}$ is the number of nuclei in the WD. The square bracket in equation (10) takes into account DM particles that scatter but do not get captured. Once captured, DM will thermalize within the WD inside a small region of size (Kouvaris & Tinyakov 2011)

$$R_{\rm th} = \left(\frac{9\, k_{\rm B}\, T_{\rm wd}}{4\pi\, G \rho_{\rm c}\, m_\chi}\right)^{1/2}$$
$$\approx 90\,{\rm m} \left(\frac{m_\chi}{10^6\,{\rm GeV}}\right)^{-1/2}\left(\frac{\rho_{\rm c}}{10^8\,{\rm g\,cm^{-3}}}\right)^{-1/2}\left(\frac{T_{\rm wd}}{10^7\,{\rm K}}\right)^{1/2} \quad (11)$$

where $T_{\rm wd}$ the WD core temperature and $\rho_{\rm c}$ is the central WD density.

The thermalized DM sphere will self-gravitate and collapse if its density surpasses that of the WD density, which requires an amount (Kouvaris & Tinyakov 2011)

$$N_{\rm sg} = \frac{4\pi\, \rho_{\rm c}\, R_{\rm th}^3}{3\, m_\chi}\,. \quad (12)$$

The self-gravitating DM sphere attracts and heats WD nuclei in its vicinity. For DM lighter than 10^8 GeV, the collapsed sphere is larger than the minimal ignition size for the WD parameters of interest (Bramante 2015). Therefore, since the temperature profile is steep, the ignition conditions of Section 2.1 are verified.

We define the time delay to ignition

$$t_{\rm i} = \frac{N_{\rm sg}}{\Gamma_{\rm cap}}\,. \quad (13)$$

Note that equation (13) depends on $M_{\rm wd}$, ρ_χ, v_χ, m_χ, $\sigma_{\chi n}$ and $T_{\rm wd}$. It can be verified easily from equation (13) that, for example, lighter WDs explode later or only in DM denser environments. Similar to the mechanism based on PBHs, fast decliners or low mass explosions are excluded in regions of low mass density due to the finite age of the universe (see Fig. 1b). Therefore, for both mechanisms we expect a triangular distribution of events in the $\rho_\chi - M_{\rm wd}$ plane.

2.3 Dark Matter environment

Galaxies are dynamical objects that grow over time and merge with other galaxies, but there are some common features: For rotationnally supported galaxies, most stars are distributed in a disk, which is immersed in a halo of dark matter. According to Kilic et al. (2019), only 1 WD in 1000 is located in the halo outside the disk. For elliptical galaxies, the disk approximation is not true. However, since elliptical galaxies contain many old SNe Ia, these are of special interest for this study. To remain as close as possible to the disk approximation, we exclude elliptical galaxies with a spherical shape, but we keep elliptical galaxies with an oblate shape that present a measureable inclination i (according to hyperLEDA), bearing in mind that systematic errors might be more important in these galaxies. We will discuss this assumption in Section 4. From the observation 69 SNe Ia

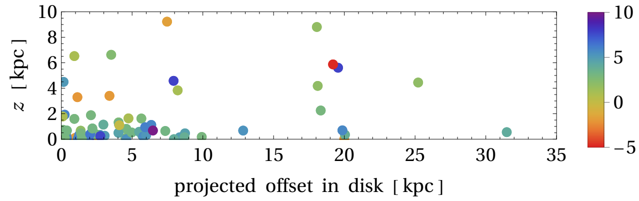

Figure 2. Supernova vertical offset $z = \sin\phi\, r_\perp$ above the disk in edge-on ($86° \leq i \leq 90°$) galaxies as a function of projected offset in disk $x = \cos\phi\, r_\perp$. The center of the host galaxy is located at $(0, 0)$ and the disk extends along the x-axis. Colors indicate Hubble type t_H of host ($t_H > 0$ = spiral, $0 > t_H > -3$ = lenticular, $t_H < -3$ = elliptical).

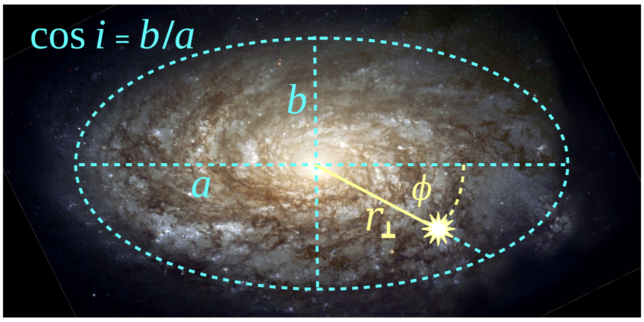

Figure 3. Schematic view of a galaxy showing the inclined disk (turquoise dashed ellipse), major and minor axes a and b (turquoise dashed lines) and the position angle ϕ and tangential offset $r_\perp$ (yellow plain line) of the SN (white star symbol). Picture credit : Hubble Space Telescope (`https://hubblesite.org/image/836/gallery`)

in edge-on galaxies ($86° \leq i \leq 90°$), we have checked that the median vertical offset z from the disk plane is as low as 0.6 kpc and that 80 per cent have $z < 2$ kpc in all types of galaxies (see Fig. 2). This is a conservative estimation, since selection effects due to dust extinction tend to obscure and hide events hidden in the disk, especially in edge-on galaxies where the dust layer in the line-of-sight is maximal.

For the range of radial offsets from galactic centers where Sne Ia occur, our method assumes that: (1) stars are contained in a disk; (2) DM particles are distributed in a spherically symmetric halo with density $\rho_\chi(r)$; (3) DM particle random velocities are locally isotropic with dispersion $v_\chi(r)$; and (4) ρ_χ and v_χ experienced by a star remain the same over its lifetime.

One of the main challenges of this study is to estimate the three-dimensional offset of the SN event from the galactic center. This distance can be decomposed in its radial (line-of-sight) and tangential (orthogonal-to-sight) components

$$r = \sqrt{r_{||}^{\,2} + r_\perp^{\,2}}\,. \tag{14}$$

The tangential part is easily determined by $r_\perp = \theta\, d$, where θ is the angular separation between the SN and the center of its host galaxy on the sky, and d the distance to the host galaxy.

In order to estimate the radial contribution $r_{||}$, let us call i the angle between the axis perpendicular to the disk and the line-of-sight and ϕ the position angle of the supernova with respect to the major axis of the inclined disk (see Fig. 3). These two angles are easy to measure. Assuming SNe in the disk, there are two special cases where the tangential distance $r_\perp$ coincides exactly with the three-dimensional distance r. The first case is for face-on disk galaxies ($i = 0$), and the second case is when the SN lies on the major axis ($\phi = 0$). In the general case it can be shown that the three-dimensional offset is given by

$$r = r_\perp \sqrt{\cos^2(\phi) + \sin^2(\phi)\,[1 + \tan^2(i)]}\,. \tag{15}$$

Here we take the following precaution: Since equation (15) diverges if i goes to 90° and $\phi \neq 0°$, we discard events where the host galaxy has an inclination within 10 per cent of 90°.

Once we know r for each SN from equation (15), we reconstruct the local DM density with the spherically symmetric density profile $\rho_\chi(r)$ from Navarro et al. (1996), where we use the halo concentration from Dutton & Macció (2014), the halo mass from the halo abundance matching from Moster et al. (2013) and the stellar mass from the mass-to-light ratio from Bell et al. (2003) using preferably K-band and if not B-band magnitudes of the host galaxies (see Table E1 and appendix A for technical details). We estimate 0.2 dex of systematic uncertainty in ρ_χ due to the use of stellar-to-mass relation and halo abundance matching. For the NFW density profile, under the assumption of local isotropy, the velocity dispersion $v_\chi(r)$ is given by equation (14) of Lokas & Mamon (2001), see also appendix C for technical details.

We take special care when choosing the distance measurements (see columns 6 to 8 in Table E1). Curiously, distance errors have a negligible effect on the estimation of ρ_χ. Consider that if we overestimated the distance, then we would overestimate the halo mass but also the offset r of the SN, which cancels out. Specifically, we have tested that for the hole range of parameters (angular separation $0.5'' < \theta < 278''$, host magnitude $1 < K < 14$, and distance $0.7\,\mathrm{Mpc} < d < 337\,\mathrm{Mpc}$) an error of 20 per cent in the estimation of the distance, induces less than 1 per cent of error in the estimation of $\log_{10}(\rho_\chi)$, with typical errors less than 0.1 per cent. Thus, we can state that the estimation of ρ_χ is almost distance-independent.

Let us briefly discuss the effects of baryonic feedback on the DM halo. The effects of SN feedback in dwarf galaxies has been studied by Di Cintio et al. (2014). Applying their prescription, 5 DM halos of the presented sample are subjected to modifications, but only 2 SN events (2012cg and 2012ht) of these 5 occur in the core region. The DM densities ρ_χ of these two events are diminished by 0.3 and 0.2 dex respectively.

It is expected that in more massive galaxies active galactic nuclei (AGN) expand the DM halo in the core region. The sample we utilize contains 17 AGNs. The amplitude of the effect is still unknown, thus we present a crude estimation. Assuming, for example, that AGN feedback efficiently flattens a core region of 5 kpc extension of halos with masses inferior to $10^{13}\,\mathrm{M}_\odot$. Then, the DM densities ρ_χ of 4 SNe (2002de, 2002bf, 1998aq and 2003cg) in the presented sample are subjected to a modification. In view of the smallness of these modifications, it is reasonable to state that the DM density estimations presented in this section are robust under baryonic feedback effects.

2.4 SN Ia data analysis

We use the complete sample of The Open Supernova Catalog[1] with the following selection criteria: (1) spectroscopically confirmed type Ia event; (2) peak and post-peak B-band photometry available for measuring the decline rate $\Delta m_{15}(B)$; (3) SN redshift z available and at most $z < 0.08$; (4) to insure the SN is part of the host galaxy, we require an independent host redshift z_g available and $|z - z_g| < 0.005$; (5) host K-band or B-band magnitude available for determining the halo mass; (6) host inclination available on HyperLEDA[2] and at most $i \leq 81°$ (see Section 2.3); and (7) SN events are excluded if the host galaxy has clear evidence of interaction (according to SIMBAD[3]). In total 224 events match these criteria.

The progenitor mass $M_{\rm wd}$ is computed from equation (1) of Scalzo et al. (2014) using equation (3) of Guy et al. (2007) and the decline rate is measured directly from the publicly available light curve if not indicated otherwise (see Table E2). We estimate 0.1 $M_\odot$ of systematic uncertainty for the use of these transformations.

The progenitor mass distribution that we obtain is comparable with that of Scalzo et al. (2014, fig. 1). However, our sample shows about 25 per cent low-mass ($< 1.0\,M_\odot$) explosions, while Scalzo et al. (2014) find less than 10 per cent. One possible reason for this difference is that our sample is limited to low-redshift events ($z < 0.08$), while the sample of Scalzo et al. (2014) also includes intermediate-redshift events (up to $z < 0.2$ and $z < 0.7$). Thus, our sample has a higher percentage of 'old' events. Another possible reason is a systematic bias introduced by the (combined) use of equation (1) of Scalzo et al. (2014) and/or equation (3) of Guy et al. (2007). The distribution of events in the $\rho_\chi - M_{\rm wd}$ plane is shown in Fig. 4.

In the absence of a technique to measure the progenitor age from light curves and spectra, we estimate $t_{\rm wd}$ from the mean local star age estimate given by the Hubble type modulated mean local star age at half-light radius and radial age gradient prescription of González Delgado et al. (2015), using equations (2) to (5) from Roche et al. (1998) to estimate the galaxy half-light radius. We have compared the estimations obtained by this method with age estimations based on local star age from Rose et al. (2019), see Fig. A1 (b). The correspondence is rather crude. In the absence of measurements for the whole sample, we decide to continue to use the estimations based on the age gradient. We emphasize that care should be taken when interpreting results based on these age estimations.

Finally, we compute the core temperature $T_{\rm wd}$ as a function of age assuming an intermediate hydrogen content of $10^{-8}\,M_\odot$ using the results of Chen & Hansen (2011). The results are presented in column 14 of Table E2.

This sample of SN Ia data is the base of the data analysis to obtain the best-fit DM parameters. We define the following χ^2 variable

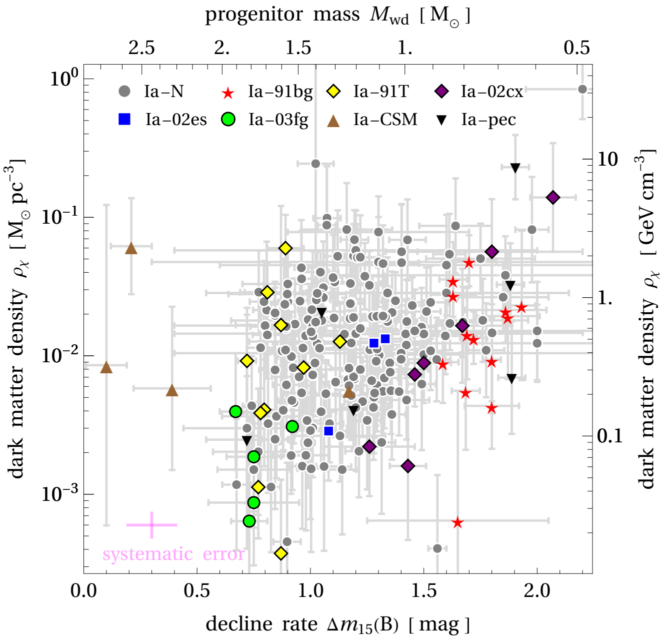

Figure 4. Archival data of 224 SN Ia events that exploded with progenitor mass $M_{\rm wd}$ and evolved in a dark matter density ρ_χ. Normal Ia events are gray disks and special Ia events according to legend. Error bars represent statistical errors. Systematic errors are shown as a light magenta cross. In the x-direction they represent additional errors on $M_{\rm wd}$ introduced by the transformation from $\Delta m_{15}(B)$. In the y-direction they represent the systematic part introduced by the halo abundance matching and the mass-to-light ratio.

$$\chi^2(\boldsymbol{p}) = \sum_j \frac{\left[t_{{\rm wd},j} - t_{\rm i}(\boldsymbol{p})_{,j}\right]^2}{\sigma_j^2}, \tag{16}$$

where $t_{{\rm wd},j}$ is the estimated age of the WD 'j' at explosion and $t_{{\rm i},j}$ the predicted time delay until ignition for WD 'j' according to equations (9) or (13) respectively. The vector $\boldsymbol{p} = (p_1, p_2)$ contains the model parameters, (m_0, σ) for PBHs and $(m_\chi, \sigma_{n\chi})$ for WIMPs. Finally, $\sigma_j^2 = \delta t_{{\rm wd},j}^2 + \delta t_{{\rm i},j}^2$ are statistical error estimates.

2.5 Progenitor channel assumptions

If the ignition of SNe Ia is triggered by an external mechanism, then not only CO WD merger remnants are potential progenitors, but also lone CO WDs. A closer inspection of the mass spectrum suggests that this is likely: as already mentioned, pure CO WDs are created in the mass range from 0.6 to 1.0 $M_\odot$. Considering that 0.2 $M_\odot$ is lost in stellar winds during the merger phase (Schwab et al. 2016), pure CO WD merger remnants are created in the mass range from 1.0 $M_\odot$ to 1.8 $M_\odot$. These two mass rages coincidentally tie-in neatly leading to the impression of an uninterrupted mass spectrum ranging from 0.6 to 1.8 $M_\odot$, as revealed by Scalzo et al. (2014).

Consequently, it is reasonable to assume that there are the following three types of progenitors that lead to SNe Ia: lone CO WDs ($0.6 < M_{\rm wd} < 1.0\,M_\odot$), CO WD merger remnants ($1.0 < M_{\rm wd} < 1.8\,M_\odot$, the DDS) and accreting WDs

[1] https://sne.space/
[2] http://leda.univ-lyon1.fr
[3] http://simbad.u-strasbg.fr/simbad/

#	DM ignition	$M_{\rm wd}$	J
1	all SNe Ia	$< 1.8\,{\rm M}_\odot$	yes
2	only sub-Chandrasekhar SNe Ia	$< 1.3\,{\rm M}_\odot$	no
3	only lone WD SNe Ia	$< 1.0\,{\rm M}_\odot$	no

Table 1. Three DM ignition assumptions reflecting possible CO WD merger remnant outcomes.

WD name	mass $[{\rm M}_\odot]$	age [yr]	ref	$\rho_\chi\,[{\rm GeV\,cm^{-3}}]$
WD 0346	0.77 ± 0.05	$(1.1 \pm 0.1) \times 10^{10}$	K12	0.43 ± 0.07
Sirius B	1.02 ± 0.01	$(1.3 \pm 0.1) \times 10^{8}$	B17	0.43 ± 0.07
WS35	> 1.49	$(1.6 \pm 0.1) \times 10^{4}$	N19	0.32 ± 0.05

Table 2. Milky Way SN Ia candidate CO WDs. References for mass and age: B17 = Bond et al. (2017), K12 = Kilic et al. (2012), N19 = Gvaramadze et al. (2019).

($M_{\rm wd} \leq 2.5\,{\rm M}_\odot$, the SDS). All have in common a CO core. Since accreting CO WDs are rare and probably correspond to the Ia-CSM sub-type, we ignore these events throughout this work, and whenever we refer to 'all events' we mean events with $M_{\rm wd} < 1.8\,{\rm M}_\odot$.

Note also that the production of radioactive ^{56}Ni requires densities heavier than $10^7\,{\rm g\,cm^{-3}}$ which is given in WDs heavier than $0.8\,{\rm M}_\odot$. Consequently, SNe Ia in the mass range from 0.6 to $0.8\,{\rm M}_\odot$ are faint and remain unobserved (van Kerkwijk et al. 2010a).

In view of the uncertainties about the outcome of the DDS stated in the introduction, we make three different hypotheses: (1) all SN Ia ($< 1.8\,{\rm M}_\odot$) ignitions are triggered by DM, (2) only sub-Chandrasekhar SN Ia ($< 1.3\,{\rm M}_\odot$) ignitions are triggered by DM, and (3) only lone WD SNe Ia ($< 1.0\,{\rm M}_\odot$) ignitions are triggered by DM. In this work we adopt sub-Chandrasekhar to be $< 1.3\,{\rm M}_\odot$. The assumptions are resumed in Table 1.

For hypothesis #1, we assume that CO WD merger remnants remain stable under rotation for at least millions of years (Tornambé & Piersanti 2013) and preserve a CO core. For this purpose, we simply assume that angular momentum J linearly increases from 0 to $2.5 \times 10^{50}\,{\rm erg\,s^{-1}}$ over the mass range from 1.0 to $1.8\,{\rm M}_\odot$. We justify this assumption by the fact that this is the minimum amount to guarantee the stability up to $1.8\,{\rm M}_\odot$ (Yoon & Langer 2005). This is the maximal DM ignition scenario.

For hypothesis #2, we assume that CO WD merger remnants slow down rapidly, on a timescale of thousands of years (Schwab et al. 2016). This time window is too small for the DM ignition mechanism presented in Section 2.2. Sub-Chandrasekhar CO WD merger remnants remain stable and are potential progenitors for DM ignition, while heavier CO WD merger remnants go SN Ia by an internal ignition mechanism. This is the intermediate DM ignition scenario.

For hypothesis #3, we assume that all SNe Ia with mass $> 1.0\,{\rm M}_\odot$ are triggered by an internal ignition mechanism and only events originating from lone CO WDs are triggered by DM. This is the minimal DM ignition scenario.

One way to test which of these three assumptions is true is to test the predicted relation between DM density ρ_χ, ejected mass $M_{\rm wd}$ and time delay to ignition $t_{\rm i}$. For this purpose, we divide the full sample in low mass ($M_{\rm wd} < 1.0\,{\rm M}_\odot$), intermediate mass ($1.0\,{\rm M}_\odot < M_{\rm wd} < 1.3\,{\rm M}_\odot$) and high mass ($1.3\,{\rm M}_\odot < M_{\rm wd} < 1.8\,{\rm M}_\odot$) sub-samples. We redivide each of these sub-samples in two equal parts, one with low DM density and one with high DM density, separated by the median $m(\rho_\chi)$ of each .

For each of these six sub-samples we compute the mean log age $\langle \log_{10} t_{\rm wd} \rangle$. It is easy to check from equations (9) and (13) that DM ignition predicts the low density part older than the high density part: $\langle \log_{10} t_{\rm i} \rangle_{<m(\rho_\chi)} > \langle \log_{10} t_{\rm i} \rangle_{>m(\rho_\chi)}$. Therefore, in each of the mass ranges where DM is supposed to be effective we must obtain

$$\langle \log_{10} t_{\rm wd} \rangle_{<m(\rho_\chi)} > \langle \log_{10} t_{\rm wd} \rangle_{>m(\rho_\chi)} \,. \tag{17}$$

2.6 Nearby white dwarf test of coherence

Any DM ignition model derived from SN Ia events can be checked for coherency by requiring that the predicted time delay to ignition of existing WDs must be larger than their actual age. We will perform this test to the best-fit models obtained with the analysis presented in Section 2.4. Since the expected mean time delay to ignition of equation (9) is probabilistic, we require for the best-fit distribution of PBHs that any existing CO WD must satisfy

$$\frac{t_{\rm wd}}{\langle t_{\rm i} \rangle} \leq O(1) \,. \tag{18}$$

Likewise, since the expected time delay to ignition of equation (13) is deterministic, we require for the best-fit WIMP model that any existing CO WD must satisfy

$$\frac{t_{\rm wd}}{t_{\rm i}} < 1 \,. \tag{19}$$

It is easy to check from equations (9) and (13) that the best candidates for SN Ia explosion are CO WDs which are old, heavy and evolve in a DM dense environment. Therefore, it is sufficient to verify the conditions (18) and (19) for a selected sample of the most extreme WDs. The candidates we choose are: WD 0346, one of the oldest known WDs; Sirius B, probably the heaviest known lone CO WD; and WS35, the heaviest and only known CO WD merger remnant (see Table 2).

To estimate the DM density of nearby WDs, we fit the Milky Way halo with an NFW profile using as calibration the distance to the galactic center $r_0 = 8.0 \pm 0.3$ (Camarillo et al. 2018) and the local DM density $\log_{10}(\rho_{\chi,0}/{\rm M}_\odot\,{\rm Mpc^{-3}}) = 16.04 \pm 0.8$ (Read 2014) and obtain the Milky Way halo mass $\log_{10}(M_{200}/{\rm M}_\odot) = 12.6 \pm 0.1$. Then we use the WD parallax and sky position to estimate its distance to the galactic center and compute the density and velocity dispersion according to the fitted NFW profile (see column 5 of Table 2).

3 RESULTS

In Section 2.2, it has been shown that DM SN Ia ignition implies that fast decliners or low mass explosions are excluded in regions of low DM density due to the finite age of the universe (see Fig. 1). The DM density measurements obtained in Section 2.3 confirm this prediction: we find a triangular distribution of events in the $\rho_\chi - M_{\rm wd}$ plane (see Fig. 4).

#	DM ignition	$\log_{10}(m_0/1\,\mathrm{g})$	σ	χ^2_{min}	dof
1	$<1.8\,\mathrm{M}_\odot$	25.2 ± 1.1	3.5 ± 1.2	479	219
2	$<1.3\,\mathrm{M}_\odot$	24.9 ± 0.9	3.3 ± 1.0	116	97
3	$<1.0\,\mathrm{M}_\odot$	~ 26	~ 6	53	53

Table 3. Best-fit parameters of a (quasi-) log-normal distribution of PBHs (bullet mechanism) obtained from the χ^2 analysis proposed in Section 2.4 and for the assumptions of Table 1. Error bars represent 68% confidence levels.

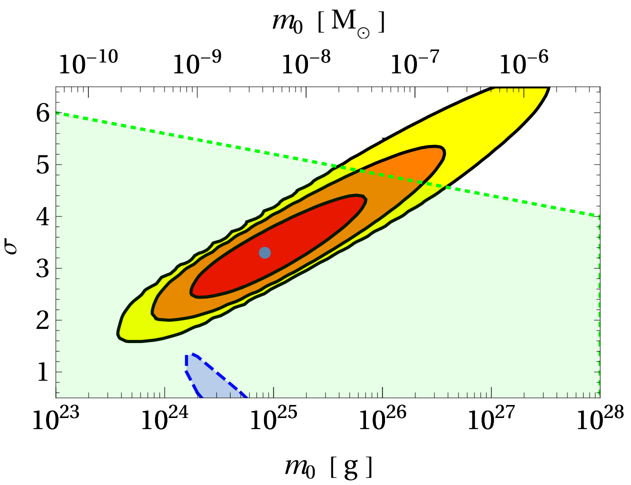

Figure 5. χ^2 analysis of the PBH mass distribution of equation (8) with peak m_0 and width σ for sub-Chandrasekhar events (assumption #2 of Section 2.5). Full line contours represent 68% (red), 95% (orange) and 99.7% (yellow) confidence regions. The dashed blue region is where 100% PBHs is permitted according to Kühnel & Freese (2017). The dotted green region is where 10% PBHs is permitted (rough extrapolation of the results of Kühnel & Freese (2017)).

Some trends of SN Ia sub-types are visible in Fig. 4: 02cx-like and 91bg-like events occur in the parameter region where DM ignitions are predicted to be old (~Gyr). Conversely, 91T-like events occur in the parameter region where DM ignitions are predicted to be young (~Myr).

We now present the results of the χ^2 analysis introduced in Section 2.4. The best-fit PBH models are presented in Table 3. For assumption #3 the values have no error estimates because the likelihood contours are open. As can be seen, for all three progenitor assumptions (see Section 2.5) the best-fit PBH mass distribution parameters are comparable. The χ^2_{min} values are comparable to the number of degrees of freedom (dof) for assumptions #2 and #3, while it is twice as large for assumption #1. For the assumption that sub-Chandrasekhar SN Ia events are triggered by DM (assumption #2), we show the degeneracy between peak m_0 and width σ in Fig. 5.

The best-fit parameters for the WIMP models are presented in Table 4. The results do not show error bars, because the value of the cross-section is unconstrained from above, since the capture rate (10) saturates at $\pi M_{\mathrm{wd}} R^2_{\mathrm{wd}}/m_n \sim 10^{-37}\mathrm{cm}^2\,(M_{\mathrm{wd}}/\mathrm{M}_\odot)^{1/3}$. Note that for this

#	DM ignition	$\log_{10}(m_\chi/1\,\mathrm{GeV})$	$\sigma_{n\chi}\,[\mathrm{cm}^2]$	χ^2_{min}	dof
1	$<1.8\,\mathrm{M}_\odot$	~ 5.5	$\sim 6\times10^{-39}$	1312	219
2	$<1.3\,\mathrm{M}_\odot$	~ 5.9	$\sim 5\times10^{-39}$	398	97
3	$<1.0\,\mathrm{M}_\odot$	~ 6.3	$\sim 4\times10^{-39}$	192	53

Table 4. Best-fit parameters of asymmetric WIMPs (poison mechanism) obtained from the χ^2 analysis proposed in Section 2.4 and for the assumptions of Table 1.

M_{wd} $[\mathrm{M}_\odot]$	$m(\rho_\chi)$ $[\mathrm{GeV\,cm^{-3}}]$	$\langle\log_{10} t_{\mathrm{wd}}\rangle_{<m(\rho_\chi)}$ [dex(yr)]	$\langle\log_{10} t_{\mathrm{wd}}\rangle_{>m(\rho_\chi)}$ [dex(yr)]
[0.6, 1.0]	0.6 ± 0.1	9.3 ± 0.2	9.6 ± 0.2
[1.0, 1.3]	0.4 ± 0.1	9.1 ± 0.3	9.5 ± 0.3
[1.3, 1.8]	0.4 ± 0.1	9.0 ± 0.3	9.5 ± 0.3

Table 5. Results of the density-mass-age test described in Section 2.5. Median DM densities $m(\rho_\chi)$ are shown in column 2. Mean ages of low DM density ($< m(\rho_\chi)$) and high DM density ($> m(\rho_\chi)$) parts of each mass range are shown in column 3 and 4.

WD name	WD 0346	Sirius B	WS35
$t_{\mathrm{wd}}/\langle t_{\mathrm{i}}\rangle$ (PBHs)	$1.2^{+0.8}_{-0.5}$	$3.4^{+1.4}_{-1.0}\times10^{-2}$	$6.3^{+2.4}_{-2.5}\times10^{-6}$
$t_{\mathrm{wd}}/t_{\mathrm{i}}$ (WIMPs)	57^{+159}_{-43}	$5.0^{+4.1}_{-2.3}\times10^{-4}$	$3.0^{+4.1}_{-2.0}\times10^{-8}$

Table 6. Ratio between the observed WD age and expected time delay to ignition as predicted by the best-fit PBH and WIMP models (assumption #1) presented in Tables 3 and 4 respectively.

model, χ^2_{min} is much larger than the number of degrees of freedom for all three assumptions.

We now present the results of the density-mass-age test proposed in Section 2.5. In Table 5 are shown the mean log ages of all six sub-samples. As can be seen, equation (17) is satisfied for none of the three mass bins: given the error bars, the probability that equation (17) is true is 12 to 17 per cent. This result requires a thorough discussion, which will be done in Section 4.

Now we present the results of the local WD coherence test explained in Section 2.6. In Table 6 are shown the ratios between the measured age and the expected time delay to ignition for the selected candidate CO WDs. Since the best-fit values are comparable between progenitor assumptions, only the results of assumption #1 are shown. We have checked that the results are comparable for assumptions #2 and #3. Clearly, 'WD 0346' is the best DM SN Ia ignition candidate. For the 'bullet mechanism', all three candidates satisfy the condition (18). Although WD 0346 satisfies it marginally, it is still satisfied. Therefore, this mechanism passes the test. For the 'poison mechanism', 'WD 0346' violates the condition (19). Therefore, this mechanism fails the coherence test.

4 DISCUSSION

In Section 3, we discussed how the particular distribution of SN Ia events in the $\rho_\chi - M_{\mathrm{wd}}$ due to the finite age of the universe is a prediction of DM ignition scenarios. However,

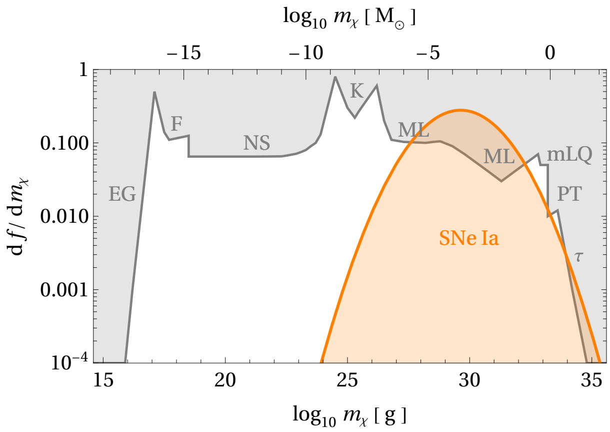

Figure 6. The differential PBH mass fraction of the best-fit (quasi-) log-normal distribution for sub-Chandrasekhar events (orange shaded region) compared with monochromatic constraints (gray shaded region): EG = extragalactic γ-rays from PBH evaporation (Carr et al. 2010), F = femtolensing of γ-ray bursts (Barnacka et al. 2012), NS = neutron star capture (Capela et al. 2013), K = Kepler microlensing of stars (Griest et al. 2014), ML = MACHO/EROS/OGLE microlensing of stars (Tisserand et al. 2007), ML = quasar microlensing (Mediavilla et al. 2009), mLQ = millilensing of quasars (Wilkinson et al. 2001), PT = pulsar timing (Schutz & Liu 2017), τ = accretion effects on the optical thickness (Ricotti et al. 2008). Figure adapted from Kühnel & Freese (2017).

due to the correlation between DM density and mean stellar age, this result alone is no proof of DM SN Ia ignition. Still, it is a motivating argument.

To compare the mass distribution of equation (8) with monochromatic constraints on PBHs, we define f as the mass fraction of DM in the form of PBHs. Its derivative with respect to mass is related to equation (8) by

$$\frac{\mathrm{d}f}{\mathrm{d}m_\chi} = N m_\chi \frac{\mathrm{d}n}{\mathrm{d}m_\chi} \tag{20}$$

where N is a normalization constant such that the integral of (20) over m_χ is equal to f. Assuming all cosmological DM made of PBHs then $f = 1$. The best-fit (quasi-) log-normal distribution is roughly in agreement with current constraints of other probes (see Fig. 6). In fact, according to the analysis of Kühnel & Freese (2017), a (quasi-) log-normal distribution of PBHs with peak $\log_{10}(m_0/1\,\mathrm{g}) \sim 24$ and width $\sigma \sim 1$ (see blue dashed region in Fig. 6) can still constitute all cosmological DM (see also Carr et al. (2016) for detailed explications on how to compare extended mass distributions with monochromatic constraints).

The best-fit asymmetric WIMP model found in this study (see Table 4) has parameters which are 2-3 orders of magnitude different from those found by Bramante (2015), who finds $m_\chi = 10^7$ GeV and $\sigma_{n\chi} = 3 \times 10^{-42}\,\mathrm{cm}^2$. One possible reason for this difference is the age dependent core temperature that we use (see Section 2.4), while Bramante (2015) uses uniformly 10^7 K, As shown in Section 2.2.2, the 'poison mechanism' is particularly sensitive to the WD core temperature, since this defines the size of the self-gravitating DM sphere. Our results are in clear tension - and the results of Bramante (2015) are in mild tension - with current direct detection constraints (Aprile et al. 2018). However, we note that there are large divergences about the capture rate in double WDs. While Brayeur & Tinyakov (2012) find that the initial capture rate is enhanced by a factor 3 to 4, Carrera (2012) finds that (for $m_\chi = 100$ GeV) the definite capture rate in binary systems is completely zero due to gravitational slingshot ejection by the binary companion during the pendulum energy loss phase. If the latter is true, then CO WD merger remnants would start to capture WIMPs only after the merger is completed.

In Section 2.3, based on the results presented in Fig. 2, we have assumed, for simplicity, that SNe Ia in all types of host galaxies with measurable inclination are distributed in the disk. This assumption is certainly less true for lenticular and elliptical host galaxies. In order to verify this assumption for a potential bias, we have performed a χ^2 analysis excluding events in lenticular and elliptical galaxies, thus keeping only those with Hubble type $t_\mathrm{H} \geq 0$ (see Table E1 column 4). For PBHs, the results for assumptions #1, #2 and #3 are $\log_{10}(m_0/1\,\mathrm{g}) = (26.2, 26.2, 29.0)$ and $\sigma = (4.5, 4.7, 14.5)$. For assumptions #1 and #2 these values are within 95 per cent confidence levels. For assumption #3 the difference is larger, but probably a side effect of low statistical power. For WIMPs, the results for assumptions #1, #2 and #3 are $m_\chi = (5.6, 6.0, 6.5)$ and $\log_{10}(\sigma_\chi/1\,\mathrm{cm}^2) = (-38, -38.2, -38.6)$. These values are very close to those found with the full sample. Therefore, for PBHs, considering only spiral galaxies, both m_0 and σ are slightly higher; for WIMPs, the best-fit values are very close to those derived from all events.

The nearby WD coherence test is reliable due to its simplicity. However, WD age measurements depend on the cooling time, which also depends on the thickness of the hydrogen layer. Therefore, WDs without a hydrogen layer (non-DAs) cool down faster. According to the 'poison mechanism', those would explode earlier, however this discussion goes beyond the scope of this study.

We have found and presented in Section 3 the result that none of the mass bins passes the density-mass-age test proposed in Section 2.5. This is a model independent result that contradicts DM SN Ia ignition. Now we discuss the credibility of this result. Given the small statistical errors, the result is significant. However, the age estimations t_wd used in this work are based on the radial age gradient of mean stellar age which implies $t_\mathrm{wd} \nearrow \Leftrightarrow r \searrow \Leftrightarrow \rho_\chi \nearrow$, while DM SN Ia ignition implies $t_\mathrm{wd} \nearrow \Leftrightarrow \rho_\chi \searrow$. Therefore, the negative result of the test could have been guessed in advance. The question here is whether SN Ia progenitor age t_wd correlates with mean stellar age or not. DM SN Ia ignition predicts that progenitors in DM dense environments ignite earlier. Therefore, due to the correlation between DM density and mean stellar age, DM SN Ia ignition predicts that SNe Ia in older stellar environments ignite earlier. In other words, DM SN Ia ignition states that the progenitor age cannot be estimated from the mean stellar age gradient. In the absence of a better technique to estimate the SN Ia progenitor age, this situation cannot be resolved. Therefore, unfortunately, the density-mass-age test remains inconclusive.

In the light of this discussion, the results based on age estimation must be treated with special care.

5 CONCLUSIONS

Our study indicates that sub-Chandrasekhar mass explosions of SNe Ia can be explained if dark matter is constituted by primordial black holes with a (quasi-) log-normal distribution of masses with peak $\log_{10}(m_0/1\,\mathrm{g}) = 24.9 \pm 0.9$ and width $\sigma = 3.3 \pm 1.0$. Furthermore, our investigation proves that this same distribution is consistent with the existence of the local population of white dwarfs, and is roughly in agreement with current constraints on primordial black holes from the literature. Therefore, we conclude that this 'bullet scenario' is a viable solution for the ignition problem of sub-Chandrasekhar SNe Ia. Furthermore, if the angular momentum loss of carbon-oxygen white dwarf merger remnants is slow enough to stabilise the core over millions of years, then roughly this same distribution can explain the ignition of all SNe Ia.

Heavy asymmetric particle dark matter with mass $m_\chi \sim 8 \times 10^5$ GeV and nuclear cross-section $\sigma_{n\chi} \sim 5 \times 10^{-39}\,\mathrm{cm}^2$ could also explain the ignition of observed SNe Ia; however, the χ^2-fit has not fully captured the data. Moreover, this scenario is in tension with the existence of the nearby population of white dwarfs, as well as with current constraints on dark matter from the literature. Therefore, we conclude that this 'poison scenario' is not a viable explanation for the ignition problem of sub-Chandrasekhar SNe Ia.

ACKNOWLEDGEMENTS

We are grateful for useful discussions with Richard Parker, Kurt Anderson, Wayne Bagget, Andrea V. Maccio, Arianna Di Cintio, Martin Barstow, Detlev Koester, Howard Bond, Simon Joyce, Benjamin Rose, and Jack Lissauer.

HS is thankful for FAPES/CAPES DCR grant n° 009/2014. SP is partly supported by the U.S.A. Department of Energy, grant number de-sc0010107. DR and VM thank CNPq and FAPES for partial financial support.

We acknowledge the usage of The Open Supernova Catalogue (https://sne.space/) HyperLeda database (http://leda.univ-lyon1.fr), NASA/IPAC Extragalactic Database (https://ned.ipac.caltech.edu/), SDSS SkyServer (http://skyserver.sdss.org/dr13/en/home.aspx) and Aladin Sky Atlas (https://aladin.u-strasbg.fr/).

REFERENCES

Acevedo J. F., Bramante J., 2019, arXiv e-prints, p. arXiv:1904.11993
Aprile E., et al., 2018, Phys. Rev. Lett., 121, 111302
Badenes C., Hughes J. P., Bravo E., Langer N., 2007, ApJ, 662, 472
Barnacka A., Glicenstein J. F., Moderski R., 2012, Phys. Rev. D, 86, 043001
Bell E. F., McIntosh D. H., Katz N., Weinberg M. D., 2003, Astrophys. J. Suppl., 149, 289
Benz W., Hills J. G., Thielemann F. K., 1989, ApJ, 342, 986
Binney J., Tremaine S., 1987, Galactic dynamics
Bond H. E., et al., 2017, ApJ, 840, 70
Bondi H., Hoyle F., 1944, MNRAS, 104, 273
Bramante J., 2015, Phys. Rev. Lett., 115, 141301
Branch D., Fisher A., Nugent P., 1993, AJ, 106, 2383
Brayeur L., Tinyakov P., 2012, Phys. Rev. Lett., 109, 061301
Bulla M., Goobar A., Dhawan S., 2018, Mon. Not. Roy. Astron. Soc., 479, 3663
Burns C. R., et al., 2018, Astrophys. J., 869, 56
Camarillo T., Mathur V., Mitchell T., Ratra B., 2018, Publ. Astron. Soc. Pac., 130, 024101
Capela F., Pshirkov M., Tinyakov P., 2013, Phys. Rev. D, 87, 023507
Carr B. J., Kohri K., Sendouda Y., Yokoyama J., 2010, Phys. Rev. D, 81, 104019
Carr B., Kühnel F., Sandstad M., 2016, Phys. Rev. D, 94, 083504
Carrera D., 2012, The effect of dark matter capture on binary stars, https://lup.lub.lu.se/student-papers/search/publication/3242612
Carvalho G. A., Marinho R. M. J., Malheiro M., 2015, in Journal of Physics Conference Series. p. 012058, doi:10.1088/1742-6596/630/1/012058
Chandrasekhar S., 1931, ApJ, 74, 81
Chen E. Y., Hansen B. M. S., 2011, MNRAS, 413, 2827
Chen P., et al., 2019, ApJ, 880, 35
Childress M. J., Filippenko A. V., Ganeshalingam M., Schmidt B. P., 2014a, Mon. Not. Roy. Astron. Soc., 437, 338
Childress M. J., Wolf C., Zahid H. J., 2014b, Mon. Not. Roy. Astron. Soc., 445, 1898
Chomiuk L., et al., 2016, ApJ, 821, 119
Cole S., Lacey C., 1996, MNRAS, 281, 716
Colgate S. A., McKee C., 1969, ApJ, 157, 623
Cox A. N., 2000, Allen's astrophysical quantities. AIP Press
Dan M., Rosswog S., Guillochon J., Ramirez-Ruiz E., 2012, MNRAS, 422, 2417
Di Cintio A., Brook C. B., Dutton A. A., MacciÃš A. V., Stinson G. S., Knebe A., 2014, Mon. Not. Roy. Astron. Soc., 441, 2986
Dutton A. A., Macció A. V., 2014, Mon. Not. Roy. Astron. Soc., 441, 3359
Gilfanov M., Bogdán Á., 2010, Nature, 463, 924
González Delgado R. M., et al., 2015, A&A, 581, A103
Gonzalez-Gaitan S., et al., 2011, Astrophys. J., 727, 107
Gould A., 1987, Astrophys. J., 321, 571
Graham P. W., Rajendran S., Varela J., 2015, Phys. Rev., D92, 063007
Graham P. W., Janish R., Narayan V., Rajendran S., Riggins P., 2018, Phys. Rev. D, 98, 115027
Green A. M., 2016, Phys. Rev. D, 94, 063530
Griest K., Cieplak A. M., Lehner M. J., 2014, ApJ, 786, 158
Guy J., et al., 2007, Astron. Astrophys., 466, 11
Gvaramadze V. V., Gräfener G., Langer N., Maryeva O. V., Kniazev A. Y., Moskvitin A. S., Spiridonova O. I., 2019, Nature, 569, 684
Hall J., Gondolo P., 2006, Phys. Rev., D74, 063511
Howell D. A., 2011, Nature Communications, 2, 350
Hoyle F., Fowler W. A., 1960, ApJ, 132, 565
Iben I. J., Tutukov A. V., 1984, ApJS, 54, 335
Janish R., Narayan V., Riggins P., 2019, Phys. Rev. D, 100, 035008
Jester S., et al., 2005, Astron. J., 130, 873
Katz B., Dong S., 2012, arXiv e-prints, p. arXiv:1211.4584
Kilic M., Thorstensen J. R., Kowalski P. M., Andrews J., 2012, MNRAS, 423, L132
Kilic M., Bergeron P., Dame K., Hambly N. C., Rowell N., Crawford C. L., 2019, mnras, 482, 965
Kippenhahn R., Weigert A., 1990, Stellar Structure and Evolution
Kouvaris C., Tinyakov P., 2011, Phys. Rev. D, 83, 083512
Kravtsov A., Vikhlinin A., Meshscheryakov A., 2018, Astron. Lett., 44, 8
Krisciunas K., et al., 2017, Astron. J., 154, 211
Kromer M., Sim S. A., Fink M., Röpke F. K., Seitenzahl I. R., Hillebrandt W., 2010, ApJ, 719, 1067
Kühnel F., Freese K., 2017, Phys. Rev. D, 95, 083508
Leonard D. C., 2007, ApJ, 670, 1275

Leung S.-C., Chu M.-C., Lin L.-M., 2015, ApJ, 812, 110
Li W., et al., 2019, Astrophys. J., 870, 12
Lissauer J. J., 1993, Ann. Rev. Astron. Astrophys., 31, 129
Lokas E. L., Mamon G. A., 2001, Mon. Not. Roy. Astron. Soc., 321, 155
Loren-Aguilar P., Isern J., Garcia-Berro E., 2009, AIP Conf. Proc., 1122, 320
Makarov D., Prugniel P., Terekhova N., Courtois H., Vauglin I., 2014, Astron. Astrophys., 570, A13
Martinsson T. P. K., Verheijen M. A. W., Westfall K. B., Bershady M. A., Andersen D. R., Swaters R. A., 2013, A&A, 557, A131
McDermott S. D., Yu H.-B., Zurek K. M., 2012, Phys. Rev., D85, 023519
Mediavilla E., et al., 2009, ApJ, 706, 1451
Mennekens N., Vanbeveren D., De Greve J. P., De Donder E., 2010, A&A, 515, A89
Montero-Camacho P., Fang X., Vasquez G., Silva M., Hirata C. M., 2019, J. Cosmology Astropart. Phys., 2019, 031
Moster B. P., Naab T., White S. D. M., 2013, Mon. Not. Roy. Astron. Soc., 428, 3121
Navarro J. F., Frenk C. S., White S. D. M., 1996, Astrophys. J., 462, 563
Nelemans G., Yungelson L. R., Portegies Zwart S. F., Verbunt F., 2001, A&A, 365, 491
Niemeyer J. C., Jedamzik K., 1999, Phys. Rev. D, 59, 124013
Niemeyer J. C., Woosley S. E., 1997, ApJ, 475, 740
Olling R. P., et al., 2015, Nature, 521, 332
Pakmor R., Kromer M., Röpke F. K., Sim S. A., Ruiter A. J., Hillebrandt W., 2010, Nature, 463, 61
Perlmutter S., et al., 1997, ApJ, 483, 565
Perlmutter S., et al., 1999, ApJ, 517, 565
Phillips M. M., 1993, ApJ, 413, L105
Pritchet C. J., Howell D. A., Sullivan M., 2008, ApJ, 683, L25
Read J. I., 2014, J. Phys., G41, 063101
Ricotti M., Ostriker J. P., Mack K. J., 2008, ApJ, 680, 829
Riess A. G., et al., 1998, AJ, 116, 1009
Riess A. G., et al., 2016, Astrophys. J., 826, 56
Roche N., Ratnatunga K., Griffiths R. E., Im M., Naim A., 1998, MNRAS, 293, 157
Rose B. M., Garnavich P. M., Berg M. A., 2019, ApJ, 874, 32
Rosswog S., Kasen D., Guillochon J., Ramirez-Ruiz E., 2009, ApJ, 705, L128
Sasaki M., Suyama T., Tanaka T., Yokoyama S., 2018, Classical and Quantum Gravity, 35, 063001
Scalzo R. A., Ruiter A. J., Sim S. A., 2014, Mon. Not. Roy. Astron. Soc., 445, 2535
Schutz K., Liu A., 2017, Phys. Rev. D, 95, 023002
Schwab J., Quataert E., Kasen D., 2016, MNRAS, 463, 3461
Seitenzahl I. R., Meakin C. A., Townsley D. M., Lamb D. Q., Truran J. W., 2009, ApJ, 696, 515
Shapiro S. L., Teukolsky S. A., 1986, Black Holes, White Dwarfs and Neutron Stars: The Physics of Compact Objects
Sim S. A., Röpke F. K., Hillebrandt W., Kromer M., Pakmor R., Fink M., Ruiter A. J., Seitenzahl I. R., 2010, ApJ, 714, L52
Stritzinger M., Mazzali P. A., Sollerman J., Benetti S., 2006, A&A, 460, 793
Taubenberger S., 2017, The Extremes of Thermonuclear Supernovae. Springer International Publishing AG, p. 317, doi:10.1007/978-3-319-21846-5_37
Thompson T. A., 2011, ApJ, 741, 82
Timmes F. X., Woosley S. E., 1992, ApJ, 396, 649
Tisserand P., et al., 2007, A&A, 469, 387
Tornambé A., Piersanti L., 2013, MNRAS, 431, 1812
Tully R. B., Courtois H. M., Sorce J. G., 2016, Astron. J., 152, 50
Vallely P. J., Tucker M. A., Shappee B. J., Brown J. S., Stanek K. Z., Kochanek C. S., 2019, arXiv e-prints, p. arXiv:1902.00037
Webbink R. F., 1984, ApJ, 277, 355
Whelan J., Iben Icko J., 1973, ApJ, 186, 1007
Wilkinson P. N., et al., 2001, Phys. Rev. Lett., 86, 584
Woods T. E., Gilfanov M., 2013, MNRAS, 432, 1640
Woosley S. E., Weaver T. A., 1986, ARA&A, 24, 205
Yoon S. C., Langer N., 2005, A&A, 435, 967
de Vaucouleurs G., Corwin Jr. H. G., 1985, ApJ, 295, 287
van Kerkwijk M. H., Chang P., Justham S., 2010a, Astrophys. J., 722, L157
van Kerkwijk M. H., Chang P., Justham S., 2010b, ApJ, 722, L157

APPENDIX A: ESTIMATION OF HALO MASSES

Given the apparent K-band magnitude m_K of a galaxy, the total luminosity of stars is

$$L_*(K) = \left(\frac{d}{1\,\mathrm{Mpc}}\right)^2 10^{0.4\left(M_{K\odot}-m_K+25\right)} \quad [\mathrm{L}_\odot], \tag{A1}$$

where d is the luminosity distance and $M_{K\odot} = 3.286$ (Cox 2000) is the absolute K-band magnitude of the sun. The total mass in stars is

$$M_* = \Upsilon_*(K)\, L_*(K) \quad [\mathrm{M}_\odot], \tag{A2}$$

where $\Upsilon_*(K) = 0.6 \pm 0.05$ according to (cite) or $\Upsilon_*(K) = 0.31 \pm 0.07$ according to Martinsson et al. (2013) is the color independent K-band mass-to-light ratio.

Alternatively, given the apparent B-band and V-band magnitudes, the total luminosity of stars $L_*(B)$ in the B-band is determined from equations analog to (A1) and (A2) with $M_{B\odot} = 5.44$ (Cox 2000) and the color dependent B-band mass-to-light ratio (Bell et al. 2003, table A7)

$$\log_{10} \Upsilon_*(B) = -0.942 + 1.737\,(B-V) \pm 0.1\,. \tag{A3}$$

In this work we use magnitudes and colors from HyperLEDA. For some rare cases, we use the the transformations of Jester et al. (2005, table 1) to convert magnitudes and colors from the ugriz to the UBV photometric systems. For galaxies where both K-band and B-band magnitudes are available, we use the K-band procedure as default. Since we find a better match between the K-band and B-band procedures (see Fig. A1) with the mass-to-light ratio from (cite), we use $\Upsilon_*(K) = 0.6 \pm 0.05$ throughout. If, instead we would use the mass-to-light ratio from Martinsson et al. (2013), the final DM density estimations vary about 0.1 dex.

Finally, we estimate the halo masses using the halo abundance matching relation M_*-M_{200} from Moster et al. (2013). If instead we would use the one of Kravtsov et al. (2018), the final DM density estimations vary about 0.1 dex. Therefore, we estimate the systematic error on the estimation of the DM density by the combined use of the mass-to-light ratio and the halo abundance matching to be 0.2 dex.

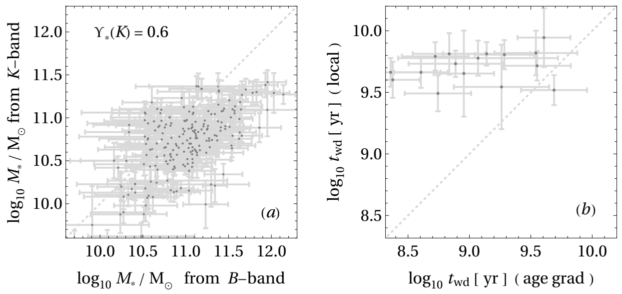

Figure A1. (a) Stellar masses of those galaxies where both K-band and B-band estimations are available; (b) SN Ia progenitor age estimated from age gradient procedure of González Delgado et al. (2015) compared to the estimation based on local star age from Rose et al. (2019).

APPENDIX B: DARK MATTER DENSITY PROFILE

The universal DM density profile is of the form (Navarro et al. 1996)

$$\rho_\chi(r) = \frac{\rho_s r_s^3}{r\,(r_s + r)^2}\,, \tag{B1}$$

where r_s and ρ_s are scaling constants determined from the halo mass M_{200} in the following way: First, the scale radius

$$r_s \equiv r_{200}/c_{200} \tag{B2}$$

is determined from the virial radius

$$r_{200} = \left(\frac{3\,M_{200}}{4\,\pi\,200\,\rho_{cr,0}}\right)^{1/3}, \tag{B3}$$

where $\rho_{cr,0} = 1.34 \times 10^{11}\,\mathrm{M_\odot\,Mpc^{-3}}$ is the critical density today, and the concentration parameter is (Dutton & Macció 2014)

$$c_{200} = 10^{0.905}\left(\frac{M_{200}}{10^{12} h^{-1} \mathrm{M_\odot}}\right)^{-0.101}, \tag{B4}$$

where $h = 0.7$ is the reduced Hubble constant. Then, the scaling density is given by

$$\rho_s = \frac{200\,\rho_{cr,0}}{3}\,c_{200}^3\,g(c_{200}), \tag{B5}$$

with the auxiliary function

$$g(x) = \frac{1}{\ln(1+x) - x/(1+x)}\,. \tag{B6}$$

APPENDIX C: DARK MATTER VELOCITY DISPERSION

Assuming DM particles distributed in a spherically symmetric density profile and in steady-state hydrodynamical equilibrium, the radial Jeans equation is

$$\frac{1}{\rho_\chi}\frac{\partial}{\partial r}(\rho_\chi\,v_{\chi r}^2) + 2\frac{(v_{\chi r}^2 - v_{\chi t}^2)}{2} = -\frac{\partial \Phi}{\partial r}\,, \tag{C1}$$

where $v_{\chi r}$ and $v_{\chi t}$ are the radial and transverse velocity dispersions and Φ is the gravitational potential. For the NFW profile given by equation (B1), the gravitational potential is (Cole & Lacey 1996)

$$\Phi(r) = -4\,\pi\,G\,\rho_s\,r_s^2\,\frac{\ln(1 + r/r_s)}{r/r_s}\,, \tag{C2}$$

where ρ_s and r_s are given by equations (B5) an (B2). Further assuming isotropic velocity dispersion ($v_{\chi t} = v_{\chi r}$), and introducing equation (C2) in equation (C1), the total square isotropic velocity dispersion is (Lokas & Mamon 2001)

$$\begin{aligned} v_\chi^2(r) = \frac{3\,G\,M_{200}\,g(c_{200})\,r}{2\,r_s^2}\left(1+\frac{r}{r_s}\right)^2 \Bigg[\pi^2 - \frac{r_s}{r} - \frac{6}{1+r/r_s} \\ - \frac{1}{(1+r/r_s)^2} + \ln\left(1+r/r_s\right)\left(1 + \frac{r_s^2}{r^2} - \frac{4\,r_s}{r} - \frac{2}{1+r/r_s}\right) \\ - \ln\left(\frac{r}{r_s}\right) + 3\ln^2(1+r/r_s) + 6\,\mathrm{Li}_2\left(-\frac{r}{r_s}\right)\Bigg], \end{aligned} \tag{C3}$$

where r_{200}, c_{200} and $g(x)$ are given by equations (B3), (B4) and (B6) and $\mathrm{Li}_2(x) = \int_x^0 [\ln(1-t)/t]\,\mathrm{d}t$ is the dilogarithm function. Strictly speaking, Lokas & Mamon (2001) derived the radial part of the isotropic velocity dispersion, $v_{\chi r}$. In this work, we are interested in the total (three-dimensional) velocity dispersion, which is $v_\chi = \sqrt{3}\,v_{\chi r}$. Therefore, equation (C3) differs from equation (14) of Lokas & Mamon (2001) by a factor 3.

APPENDIX D: WHITE DWARF PARAMETERS

The WD mass is given by (Scalzo et al. 2014)

$$M_{wd} = (1.32 \pm 0.02) + (1.89 \pm 0.02)\,x_1 \tag{D1}$$

where x_1 is the SALT2 stretch parameter which is related to the B-band post-peak decline rate by (Perlmutter et al. 1997)

$$\Delta m_{15}(B) = 1.09 - 0.161\,x_1 + 0.013\,x_1^2 - 0.0013\,x_1^3\,. \tag{D2}$$

The WD central density ρ_c depends on the WD mass and its total angular momentum J. For densities $\rho_c > 10^7\,\mathrm{g\,cm^{-3}}$, the following relation has been determined (Yoon & Langer 2005, equations 19 to 22)

$$\begin{aligned} J(M_{wd}, \rho_c) = C_1(\rho_c)\left[1 - \exp\left(-\,0.2\,[M_{wd} - M_{nr}(\rho_c)]^{0.48}\right)\right] \\ + C_2(\rho_c)\left[M_{wd} - M_{nr}(\rho_c)\right]^{1.3}\,[10^{50}\,\mathrm{erg\,s}], \end{aligned} \tag{D3}$$

with

$$C_1(\rho_c) = 20.800370 - 1.5856256\,\log_{10}(\rho_c),$$
$$C_2(\rho_c) = 11.397626 - 0.97306637\,\log_{10}(\rho_c),$$

and the non-rotating mass

$$\begin{aligned} M_{nr}(\rho_c) = 1.436\Big[1 - \exp\Big(-\,0.01316\,(\log_{10}\rho_c)^{2.706} \\ + 0.2493\,\log_{10}\rho_c\Big)\Big]\,. \end{aligned} \tag{D4}$$

For non-rotating WDs, equation (D4) can be used directly. For progenitor assumption #1 (see Sec. 2.5), we assume that angular momentum increases linearly from $J = 0$ ($M_{wd} = 1.0\,\mathrm{M_\odot}$) to $J = 2.5 \times 10^{51}\,\mathrm{erg\,s^{-1}}$ ($M_{wd} = 1.8\,\mathrm{M_\odot}$).

The WD radius $R_{\rm wd}$ can be calculated with the fitting formula (Carvalho et al. 2015, equation 9)

$$M_{\rm wd} = \left(a\,R_{\rm wd} + b\right)\left[\,\exp(c\,R_{\rm wd}^{2}) + d\right]^{-1} \quad [\mathrm{M}_\odot] \tag{D5}$$

where $a = 2.325{\times}10^{-5}\,\mathrm{km}^{-1}$, $b = 0.4617$, $c = 7.277{\times}10^{-9}\,\mathrm{km}^{-2}$ and $d = -0.644$ and $R_{\rm wd}$ is in km. Equation (D5) is valid down to $R_{\rm wd} > 17\,000\,\mathrm{km}$ or, equivalently, up to $M_{\rm wd} < 1.33\,\mathrm{M}_\odot$. For progenitor assumption #1 (see Sec. 2.5), we compute first the central density using equation (D3), then we compute the radius with equation (D5) assuming the mass of a non-rotating WD with the same central density, that is from equation (D4).

APPENDIX E: DATA INFORMATION

In the following two Tables are presented the data. In Table E1 we specify SN Ia host information. In Table E2 we specify particular SN Ia information.

Table E1: Global SN host galaxy information

ID	SN name	host name	Hubble type	z	μ [mag]	method	ref	i [°]	$\log_{10}(M_*)$ [dex(M$_\odot$)]	$\log_{10}(M_{200})$ [dex(M$_\odot$)]
1	1885A	M31	3.0 ± 0.4	0.0000	24.40 ± 0.12	CTLS	T16	72	10.5 ± 0.1	11.9 ± 0.4
2	1939A	NGC 4636	-4.8 ± 0.5	0.0031	30.90 ± 0.24	SF	T16	64	10.9 ± 0.2	12.7 ± 0.7
3	1939B	M59	-4.8 ± 0.4	0.0030	30.90 ± 0.24	SF	T16	72	10.8 ± 0.2	12.4 ± 0.7
4	1980N	NGC 1316	-1.8 ± 0.7	0.0059	31.20 ± 0.15	SNF	T16	65	11.3 ± 0.1	13.9 ± 0.6
5	1981B	NGC 4536	4.3 ± 0.7	0.0060	30.90 ± 0.05	C	R16	77	10.4 ± 0.1	11.9 ± 0.4
6	1981D	NGC 1316	-1.8 ± 0.7	0.0059	31.20 ± 0.15	SNF	T16	65	11.3 ± 0.1	13.9 ± 0.6
7	1986A	NGC 3367	5.1 ± 0.6	0.0100	33.30 ± 0.35	M	M14	48	10.9 ± 0.2	12.8 ± 0.8
8	1986G	NGC 5128	-2.1 ± 0.6	0.0012	27.80 ± 0.12	CTLS	T16	70	10.6 ± 0.1	12.2 ± 0.6
9	1989A	NGC 3687	3.8 ± 0.7	0.0084	32.90 ± 0.41	M	M14	27	10.4 ± 0.2	11.8 ± 0.6
10	1989B	NGC 3627	3.1 ± 0.4	0.0024	29.80 ± 0.13	CTHI	T16	60	10.6 ± 0.1	12.2 ± 0.5
11	1990N	NGC 4639	3.6 ± 0.7	0.0034	31.50 ± 0.07	C	R16	49	10.2 ± 0.1	11.6 ± 0.4
12	1991bg	NGC 4374	-4.4 ± 1.2	0.0035	31.10 ± 0.15	SNF	T16	32	11.0 ± 0.1	13.1 ± 0.6
13	1991T	NGC 4527	4.0 ± 0.2	0.0058	30.60 ± 0.17	CHI	T16	79	10.6 ± 0.1	12.1 ± 0.5
14	1992al	PGC 65335	5.1 ± 0.5	0.0140	33.70 ± 0.17	N	T16	79	10.2 ± 0.2	11.6 ± 0.4
15	1992bo	PGC 4972	-1.5 ± 1.4	0.0185	34.50 ± 0.17	N	T16	60	10.5 ± 0.1	12.0 ± 0.5
16	1993H	PGC 49304	1.9 ± 0.5	0.0242	34.80 ± 0.17	N	T16	18	10.7 ± 0.2	12.4 ± 0.7
17	1994ae	NGC 3370	5.1 ± 1.1	0.0043	32.10 ± 0.05	C	R16	68	10.1 ± 0.1	11.6 ± 0.4
18	1994S	NGC 4495	2.1 ± 0.6	0.0152	34.00 ± 0.17	N	T16	69	10.6 ± 0.1	12.1 ± 0.5
19	1995ak	IC 1844	4.0 ± 2.0	0.0227	34.50 ± 0.15	NHI	T16	68	10.3 ± 0.1	11.8 ± 0.4
20	1995al	NGC 3021	4.0 ± 0.2	0.0068	32.50 ± 0.09	C	R16	60	10.4 ± 0.1	11.8 ± 0.4
21	1995bd	UGC 3151	4.0 ± 2.0	0.0151	33.70 ± 0.17	N	T16	76	10.6 ± 0.1	12.1 ± 0.5
22	1995D	NGC 2962	-1.0 ± 0.7	0.0066	32.50 ± 0.20	N	T16	50	10.6 ± 0.1	12.1 ± 0.5
23	1995E	NGC 2441	3.3 ± 0.9	0.0116	33.30 ± 0.17	N	T16	3	10.4 ± 0.1	11.8 ± 0.5
24	1996bl	PGC 1392929	4.0 ± 1.5	0.0349	35.70 ± 0.17	N	T16	25	10.5 ± 0.1	12.0 ± 0.5
25	1996bo	NGC 673	5.3 ± 0.6	0.0173	33.90 ± 0.15	NHI	T16	48	10.8 ± 0.1	12.5 ± 0.6
26	1997bp	NGC 4680	0.3 ± 1.5	0.0083	32.40 ± 0.16	NH	T16	55	10.1 ± 0.1	11.6 ± 0.4
27	1997bq	NGC 3147	3.9 ± 0.5	0.0099	33.00 ± 0.17	N	T16	22	11.3 ± 0.1	13.8 ± 0.6
28	1997do	UGC 3845	3.7 ± 0.6	0.0101	33.10 ± 0.15	NHI	T16	45	10.0 ± 0.2	11.5 ± 0.4
29	1997E	NGC 2258	-2.0 ± 0.4	0.0135	33.80 ± 0.17	N	T16	45	11.3 ± 0.1	13.8 ± 0.6
30	1998ab	NGC 4704	3.8 ± 0.6	0.0272	34.90 ± 0.17	N	T16	4	10.7 ± 0.1	12.4 ± 0.6
31	1998aq	NGC 3982	3.2 ± 0.6	0.0037	31.70 ± 0.07	C	R16	20	10.2 ± 0.1	11.7 ± 0.4
32	1998bp	NGC 6495	-4.9 ± 0.4	0.0104	33.00 ± 0.17	N	T16	65	10.5 ± 0.1	11.9 ± 0.5
33	1998bu	NGC 3368	2.1 ± 0.7	0.0030	30.10 ± 0.15	CSHI	T16	52	10.6 ± 0.1	12.1 ± 0.5
34	1998de	NGC 252	-1.2 ± 0.7	0.0166	34.10 ± 0.17	N	T16	35	11.1 ± 0.1	13.3 ± 0.6
35	1998dh	NGC 7541	4.7 ± 0.9	0.0089	32.50 ± 0.15	NHI	T16	72	10.8 ± 0.1	12.4 ± 0.5
36	1998ef	UGC 646	2.5 ± 1.3	0.0177	33.90 ± 0.15	NHI	T16	72	10.5 ± 0.1	11.9 ± 0.5
37	1998es	NGC 632	-1.3 ± 1.7	0.0106	32.80 ± 0.17	N	T16	32	10.2 ± 0.1	11.6 ± 0.4
38	1999aa	NGC 2595	5.0 ± 0.4	0.0144	34.00 ± 0.17	N	T16	22	10.8 ± 0.2	12.6 ± 0.7
39	1999ac	NGC 6063	5.8 ± 0.5	0.0105	33.10 ± 0.15	NHI	T16	40	10.1 ± 0.1	11.5 ± 0.4
40	1999bh	NGC 3435	3.0 ± 0.4	0.0172	34.90 ± 0.40	H	T16	54	10.8 ± 0.2	12.4 ± 0.8
41	1999by	NGC 2841	2.9 ± 0.5	0.0021	30.80 ± 0.14	CNH	T16	68	11.0 ± 0.1	13.0 ± 0.6
42	1999cc	NGC 6038	5.1 ± 0.7	0.0313	35.50 ± 0.17	N	T16	42	11.2 ± 0.1	13.5 ± 0.7
43	1999cl	NGC 4501	3.3 ± 0.6	0.0076	31.50 ± 0.30	HI	T16	62	11.2 ± 0.2	13.5 ± 0.8
44	1999cp	NGC 5468	6.0 ± 0.3	0.0098	33.20 ± 0.17	N	T16	15	10.2 ± 0.2	11.7 ± 0.5
45	1999dk	UGC 1087	5.3 ± 0.6	0.0150	33.90 ± 0.16	NH	T16	14	10.2 ± 0.2	11.6 ± 0.4
46	1999dq	NGC 976	4.1 ± 0.6	0.0143	33.30 ± 0.16	NH	T16	21	10.8 ± 0.1	12.4 ± 0.6
47	1999ee	IC 5179	4.0 ± 0.2	0.0114	33.10 ± 0.15	NHI	T16	69	10.9 ± 0.1	12.8 ± 0.6
48	1999ej	NGC 495	0.2 ± 0.9	0.0137	34.10 ± 0.17	N	T16	42	10.7 ± 0.1	12.4 ± 0.6
49	1999ek	UGC 3329	4.1 ± 0.8	0.0175	34.10 ± 0.15	NHI	T16	72	10.8 ± 0.1	12.6 ± 0.6
50	1999gh	NGC 2986	-4.7 ± 0.6	0.0077	32.40 ± 0.17	NFP	T16	52	11.0 ± 0.1	13.0 ± 0.6
51	2000cn	UGC 11064	5.9 ± 0.4	0.0235	34.90 ± 0.17	N	T16	7	11.0 ± 0.2	13.0 ± 0.7
52	2000cw	PGC 72411	4.2 ± 2.5	0.0301	35.10 ± 0.30	HI	T16	63	10.7 ± 0.2	12.3 ± 0.7
53	2000cx	NGC 524	-1.2 ± 0.6	0.0080	31.90 ± 0.28	S	T16	4	11.0 ± 0.2	13.0 ± 0.7
54	2000E	NGC 6951	3.9 ± 0.6	0.0052	31.40 ± 0.20	N	T16	44	10.7 ± 0.2	12.3 ± 0.7
55	2001ah	UGC 6211	4.1 ± 0.5	0.0578	36.80 ± 0.17	N	T16	19	11.1 ± 0.2	13.2 ± 0.8
56	2001ba	PGC 36028	3.8 ± 0.6	0.0294	35.50 ± 0.16	NH	T16	20	11.1 ± 0.1	13.2 ± 0.6
57	2001bt	IC 4830	3.9 ± 0.5	0.0146	33.50 ± 0.16	NFP	T16	31	10.9 ± 0.1	12.7 ± 0.6
58	2001cj	UGC 8399	3.0 ± 0.4	0.0242	35.40 ± 0.03	M	M14	12	10.6 ± 0.1	12.2 ± 0.4
59	2001cz	NGC 4679	4.9 ± 0.6	0.0154	33.80 ± 0.15	NHI	T16	75	10.8 ± 0.1	12.6 ± 0.6
60	2001da	NGC 7780	2.0 ± 0.4	0.0172	34.10 ± 0.16	NH	T16	71	10.5 ± 0.1	12.0 ± 0.5
61	2001dl	UGC 11725	8.1 ± 0.4	0.0207	35.30 ± 0.25	M	M14	78	10.6 ± 0.2	12.1 ± 0.6
62	2001eh	UGC 1162	3.0 ± 0.4	0.0370	35.80 ± 0.17	N	T16	9	11.1 ± 0.2	13.3 ± 0.7
63	2001ep	NGC 1699	3.1 ± 0.6	0.0130	33.50 ± 0.17	N	T16	50	10.2 ± 0.1	11.7 ± 0.4

Continued on next page

Table E1 – *Continued from previous page*

ID	SN name	host name	Hubble type	z	μ [mag]	method	ref	i [°]	$\log_{10}(M_*)$ [dex(M$_\odot$)]	$\log_{10}(M_{200})$ [dex(M$_\odot$)]
64	2001gb	IC 582	3.2 ± 2.1	0.0257	35.20 ± 0.17	N	T16	13	10.8 ± 0.1	12.5 ± 0.6
65	2002bf	PGC 29953	3.0 ± 0.6	0.0242	34.90 ± 0.17	N	T16	44	10.7 ± 0.1	12.2 ± 0.6
66	2002bo	NGC 3190	0.9 ± 0.6	0.0054	31.70 ± 0.17	N	T16	73	10.8 ± 0.1	12.5 ± 0.6
67	2002cd	NGC 6916	4.0 ± 0.3	0.0103	33.20 ± 0.18	NH	T16	52	10.7 ± 0.1	12.2 ± 0.5
68	2002cf	NGC 4786	−4.3 ± 0.5	0.0155	33.70 ± 0.50	P	T16	55	11.1 ± 0.3	13.2 ± 0.9
69	2002cr	NGC 5468	6.0 ± 0.3	0.0098	33.20 ± 0.17	N	T16	4	10.2 ± 0.2	11.7 ± 0.5
70	2002cs	NGC 6702	−4.9 ± 0.4	0.0158	33.60 ± 0.28	S	T16	42	10.8 ± 0.2	12.6 ± 0.7
71	2002cx	PGC 45981	5.1 ± 2.6	0.0240	36.10 ± 0.03	M	M14	79	10.2 ± 0.1	11.6 ± 0.4
72	2002de	NGC 6104	3.0 ± 2.4	0.0281	35.30 ± 0.17	N	T16	39	10.9 ± 0.1	12.9 ± 0.6
73	2002do	PGC 63832	−5.0 ± 0.5	0.0159	34.10 ± 0.17	N	T16	43	11.1 ± 0.1	13.3 ± 0.6
74	2002dp	NGC 7678	4.9 ± 0.5	0.0116	33.20 ± 0.17	N	T16	27	10.7 ± 0.1	12.4 ± 0.6
75	2002eb	PGC 68560	2.0 ± 2.0	0.0275	35.50 ± 0.04	M	M14	38	10.7 ± 0.1	12.3 ± 0.5
76	2002ef	NGC 7761	−2.0 ± 0.5	0.0240	33.70 ± 0.50	P	T16	33	10.7 ± 0.3	12.3 ± 0.8
77	2002el	NGC 6986	−2.8 ± 0.8	0.0287	35.40 ± 0.04	M	M14	62	11.2 ± 0.1	13.5 ± 0.5
78	2002er	UGC 10743	1.0 ± 0.5	0.0086	32.40 ± 0.17	NHI	T16	73	9.9 ± 0.1	11.4 ± 0.4
79	2002es	UGC 2708	−2.0 ± 0.4	0.0284	34.50 ± 0.17	N	T16	12	11.2 ± 0.3	13.4 ± 1.1
80	2002fb	NGC 759	−4.8 ± 0.4	0.0156	34.10 ± 0.17	NF	T16	26	11.1 ± 0.1	13.2 ± 0.6
81	2002fk	NGC 1309	3.9 ± 0.6	0.0071	32.50 ± 0.06	C	R16	5	10.5 ± 0.1	11.9 ± 0.4
82	2002G	PGC 45498	−3.5 ± 2.1	0.0337	35.80 ± 0.17	N	T16	37	11.0 ± 0.1	12.9 ± 0.6
83	2002ha	NGC 6962	1.7 ± 0.6	0.0140	33.80 ± 0.15	NHI	T16	42	11.1 ± 0.1	13.3 ± 0.6
84	2002hw	UGC 52	5.3 ± 0.6	0.0175	34.30 ± 0.17	N	T16	20	10.6 ± 0.1	12.2 ± 0.6
85	2002ic	A013002+2153	9.5 ± 1.0	0.0660	37.20 ± 0.20	M	M14	60	9.3 ± 0.8	11.1 ± 0.7
86	2002jy	NGC 477	5.0 ± 0.4	0.0203	34.70 ± 0.16	NH	T16	65	10.8 ± 0.2	12.5 ± 0.8
87	2003cg	NGC 3169	1.2 ± 0.5	0.0041	31.80 ± 0.20	N	T16	40	10.9 ± 0.1	12.8 ± 0.6
88	2003cq	NGC 3978	3.8 ± 0.6	0.0333	35.70 ± 0.17	N	T16	3	11.4 ± 0.1	14.0 ± 0.7
89	2003du	UGC 9391	8.1 ± 0.5	0.0064	32.90 ± 0.06	C	R16	41	9.5 ± 0.1	11.2 ± 0.4
90	2003fa	PGC 60771	2.7 ± 3.0	0.0060	35.90 ± 0.17	N	T16	60	10.9 ± 0.2	12.7 ± 0.7
91	2003gn	PGC 69160	4.0 ± 0.3	0.0345	36.20 ± 0.15	M	M14	72	10.9 ± 0.1	12.7 ± 0.6
92	2003gq	NGC 7407	4.7 ± 0.9	0.0215	35.20 ± 0.40	H	T16	63	11.0 ± 0.2	13.0 ± 0.9
93	2003he	PGC 73123	4.0 ± 0.6	0.0255	35.10 ± 0.40	H	T16	73	10.6 ± 0.3	12.0 ± 0.7
94	2003W	UGC 5234	5.4 ± 1.1	0.0201	34.50 ± 0.17	N	T16	47	10.8 ± 0.1	12.4 ± 0.6
95	2003Y	IC 522	−1.9 ± 0.5	0.0169	34.20 ± 0.04	M	M14	38	10.8 ± 0.1	12.4 ± 0.5
96	2004at	PGC 33043	3.6 ± 2.2	0.0231	35.20 ± 0.03	M	M14	69	10.9 ± 0.3	12.7 ± 1.0
97	2004bg	UGC 6363	6.0 ± 0.5	0.0210	34.70 ± 0.17	N	T16	81	10.5 ± 0.1	12.0 ± 0.5
98	2004bk	NGC 5246	3.1 ± 0.4	0.0231	35.20 ± 0.04	M	M14	6	10.7 ± 0.1	12.4 ± 0.5
99	2004bw	PGC 53750	5.9 ± 0.6	0.0212	35.10 ± 0.10	M	M14	29	10.7 ± 0.2	12.4 ± 0.8
100	2004dt	NGC 799	1.1 ± 0.6	0.0193	34.50 ± 0.04	M	M14	29	10.8 ± 0.1	12.6 ± 0.5
101	2004ef	UGC 12158	3.1 ± 0.4	0.0304	35.40 ± 0.17	N	T16	2	10.8 ± 0.2	12.6 ± 0.7
102	2004eo	NGC 6928	2.0 ± 0.2	0.0152	33.80 ± 0.17	N	T16	77	11.1 ± 0.1	13.4 ± 0.6
103	2004ey	UGC 11816	4.3 ± 0.5	0.0152	34.00 ± 0.17	N	T16	10	10.1 ± 0.1	11.6 ± 0.4
104	2004fz	NGC 783	5.3 ± 0.6	0.0173	33.90 ± 0.04	M	M14	42	10.8 ± 0.1	12.5 ± 0.5
105	2004gs	PGC 24286	−3.6 ± 1.5	0.0271	35.40 ± 0.17	N	T16	35	10.8 ± 0.1	12.6 ± 0.6
106	2004L	PGC 30719	4.9 ± 2.3	0.0323	35.70 ± 0.17	N	T16	5	10.6 ± 0.2	12.1 ± 0.6
107	2005A	NGC 958	4.9 ± 0.5	0.0187	34.30 ± 0.15	NHIFP	T16	71	11.3 ± 0.1	13.7 ± 0.6
108	2005ag	PGC 200171	3.6 ± 3.0	0.0794	37.60 ± 0.17	N	T16	38	11.1 ± 0.1	13.4 ± 0.6
109	2005al	NGC 5304	−3.2 ± 1.1	0.0128	34.00 ± 0.15	NFP	T16	50	10.9 ± 0.1	12.7 ± 0.6
110	2005am	NGC 2811	1.1 ± 0.4	0.0083	32.20 ± 0.16	NFP	T16	70	10.8 ± 0.1	12.5 ± 0.6
111	2005bg	PGC 39401	3.4 ± 2.8	0.0236	35.00 ± 0.17	N	T16	9	10.3 ± 0.1	11.7 ± 0.4
112	2005bo	NGC 4708	2.1 ± 0.8	0.0145	33.80 ± 0.17	N	T16	40	10.5 ± 0.1	12.0 ± 0.5
113	2005cc	NGC 5383	3.1 ± 0.5	0.0074	32.80 ± 0.44	M	M14	21	10.8 ± 0.3	12.4 ± 0.9
114	2005de	UGC 11097	6.0 ± 1.4	0.0152	34.50 ± 0.03	M	M14	74	10.7 ± 0.1	12.3 ± 0.4
115	2005el	NGC 1819	−2.0 ± 0.4	0.0149	33.90 ± 0.17	N	T16	40	11.0 ± 0.1	12.9 ± 0.6
116	2005eq	PGC 11767	1.4 ± 4.0	0.0287	35.40 ± 0.17	NI	T16	73	10.9 ± 0.2	12.8 ± 0.7
117	2005gj	SDSS J030111.99-003313.5	4.5 ± 0.5	0.0616	37.50 ± 0.88	M	M14	79	9.0 ± 0.9	11.0 ± 0.7
118	2005hc	PGC 7299	4.4 ± 2.5	0.0450	36.40 ± 0.17	N	T16	50	10.8 ± 0.1	12.7 ± 0.7
119	2005hk	UGC 272	6.5 ± 0.8	0.0130	33.90 ± 0.30	HI	T16	67	9.5 ± 0.2	11.2 ± 0.4
120	2005iq	PGC 73098	2.0 ± 1.4	0.0335	35.80 ± 0.17	N	T16	60	10.7 ± 0.1	12.3 ± 0.6
121	2005ir	PGC 3116670	−2.1 ± 4.6	0.0753	37.60 ± 0.17	N	T16	40	10.6 ± 0.3	12.1 ± 0.8
122	2005kc	NGC 7311	2.0 ± 0.3	0.0147	33.90 ± 0.17	N	T16	59	11.1 ± 0.1	13.2 ± 0.6
123	2005ke	NGC 1371	1.1 ± 0.3	0.0047	32.30 ± 0.30	HI	T16	42	11.0 ± 0.2	12.9 ± 0.8
124	2005ki	NGC 3332	−2.7 ± 1.0	0.0192	34.60 ± 0.17	N	T16	32	11.2 ± 0.1	13.4 ± 0.6
125	2005M	NGC 2930	4.4 ± 2.7	0.0225	35.00 ± 0.17	N	T16	60	10.3 ± 0.2	11.7 ± 0.4
126	2005mc	UGC 4414	0.2 ± 0.8	0.0256	35.20 ± 0.17	N	T16	18	10.9 ± 0.1	12.8 ± 0.6
127	2005ms	UGC 4614	3.0 ± 1.8	0.0252	35.20 ± 0.17	N	T16	8	10.7 ± 0.2	12.2 ± 0.6

Continued on next page

Table E1 – *Continued from previous page*

ID	SN name	host name	Hubble type	z	μ [mag]	method	ref	i [°]	$\log_{10}(M_*)$ [dex(M$_\odot$)]	$\log_{10}(M_{200})$ [dex(M$_\odot$)]
128	2005na	UGC 3634	1.0 ± 0.4	0.0266	35.10 ± 0.17	N	T16	51	11.1 ± 0.1	13.3 ± 0.6
129	2005W	NGC 691	4.0 ± 0.2	0.0089	32.90 ± 0.30	HI	T16	51	10.7 ± 0.2	12.4 ± 0.7
130	2006ac	NGC 4619	3.1 ± 0.5	0.0231	34.90 ± 0.17	N	T16	5	11.1 ± 0.1	13.2 ± 0.6
131	2006ax	NGC 3663	3.9 ± 0.5	0.0167	34.30 ± 0.16	NFP	T16	32	10.8 ± 0.2	12.6 ± 0.7
132	2006az	NGC 4172	2.0 ± 2.0	0.0309	35.50 ± 0.17	N	T16	30	11.3 ± 0.1	13.9 ± 0.6
133	2006bh	NGC 7329	3.6 ± 1.0	0.0106	33.30 ± 0.15	NHI	T16	42	10.9 ± 0.1	12.7 ± 0.6
134	2006bq	NGC 6685	-3.0 ± 0.5	0.0219	34.80 ± 0.17	N	T16	53	10.9 ± 0.1	12.7 ± 0.6
135	2006br	NGC 5185	3.0 ± 0.4	0.0251	35.50 ± 0.18	NH	T16	74	11.2 ± 0.1	13.5 ± 0.6
136	2006bt	PGC 56443	-0.2 ± 1.0	0.0322	35.60 ± 0.17	N	T16	28	11.1 ± 0.1	13.2 ± 0.6
137	2006cp	UGC 7357	5.3 ± 0.6	0.0223	34.70 ± 0.17	N	T16	15	10.1 ± 0.2	11.5 ± 0.4
138	2006D	PGC 43690	2.1 ± 0.7	0.0089	32.80 ± 0.17	N	T16	40	10.0 ± 0.1	11.5 ± 0.4
139	2006ef	NGC 809	-1.7 ± 0.7	0.0174	34.40 ± 0.17	N	T16	45	10.6 ± 0.1	12.1 ± 0.5
140	2006em	NGC 911	-4.8 ± 0.6	0.0192	34.50 ± 0.46	F	T16	75	10.9 ± 0.2	12.9 ± 0.9
141	2006en	PGC 70600	5.0 ± 2.0	0.0319	35.60 ± 0.17	N	T16	11	11.0 ± 0.1	13.1 ± 0.6
142	2006et	NGC 232	1.1 ± 0.5	0.0217	34.60 ± 0.17	N	T16	47	11.0 ± 0.1	12.9 ± 0.6
143	2006gr	UGC 12071	3.1 ± 0.5	0.0346	35.80 ± 0.17	N	T16	41	11.6 ± 0.2	14.5 ± 0.9
144	2006gz	IC 1277	5.8 ± 0.6	0.0280	35.50 ± 0.13	M	M14	48	10.5 ± 0.2	12.0 ± 0.6
145	2006hb	PGC 16595	-3.2 ± 1.2	0.0153	33.70 ± 0.17	NFP	T16	55	10.5 ± 0.1	11.9 ± 0.5
146	2006mr	NGC 1316	-1.8 ± 0.7	0.0055	31.20 ± 0.15	SNF	T16	64	11.3 ± 0.1	13.9 ± 0.6
147	2006ob	UGC 1333	2.9 ± 0.7	0.0589	36.90 ± 0.17	N	T16	44	11.3 ± 0.1	13.8 ± 0.7
148	2006ot	PGC 8610	1.4 ± 1.3	0.0526	36.60 ± 0.16	NFP	T16	65	11.4 ± 0.2	14.0 ± 0.7
149	2006S	UGC 7934	1.5 ± 3.5	0.0321	35.80 ± 0.17	N	T16	69	10.6 ± 0.1	12.1 ± 0.6
150	2006X	M100	4.0 ± 0.3	0.0053	30.70 ± 0.12	CNH	T16	24	10.7 ± 0.2	12.3 ± 0.7
151	2007A	NGC 105	1.7 ± 0.7	0.0169	34.10 ± 0.17	N	T16	40	10.6 ± 0.1	12.1 ± 0.5
152	2007af	NGC 5584	5.9 ± 0.3	0.0055	31.80 ± 0.05	C	R16	40	9.0 ± 0.2	11.0 ± 0.4
153	2007ax	NGC 2577	-2.9 ± 0.5	0.0072	32.50 ± 0.51	M	M14	74	10.4 ± 0.3	11.9 ± 0.6
154	2007ba	UGC 9798	-0.1 ± 0.4	0.0387	36.40 ± 0.20	N	T16	70	11.4 ± 0.2	14.0 ± 0.7
155	2007bc	UGC 6332	1.0 ± 0.4	0.0211	34.70 ± 0.17	N	T16	23	10.9 ± 0.2	12.7 ± 0.7
156	2007bd	UGC 4455	1.0 ± 0.4	0.0315	35.50 ± 0.16	NFP	T16	42	10.9 ± 0.2	12.8 ± 0.7
157	2007bj	NGC 6172	-4.2 ± 0.8	0.0167	34.60 ± 0.13	M	M14	13	11.0 ± 0.1	13.0 ± 0.6
158	2007bm	NGC 3672	5.0 ± 0.4	0.0066	32.20 ± 0.17	NHI	T16	67	10.6 ± 0.1	12.2 ± 0.5
159	2007ci	NGC 3873	-4.9 ± 0.4	0.0181	34.40 ± 0.17	NF	T16	28	10.9 ± 0.1	12.8 ± 0.6
160	2007F	UGC 8162	5.9 ± 0.7	0.0236	35.10 ± 0.17	N	T16	1	10.2 ± 0.2	11.6 ± 0.4
161	2007hj	NGC 7461	-1.9 ± 0.5	0.0137	33.80 ± 0.05	M	M14	34	10.6 ± 0.1	12.1 ± 0.4
162	2007kk	UGC 2828	3.2 ± 0.4	0.0410	36.10 ± 0.20	N	T16	32	11.3 ± 0.1	13.8 ± 0.6
163	2007le	NGC 7721	4.9 ± 0.5	0.0061	31.50 ± 0.30	HI	T16	81	10.2 ± 0.2	11.6 ± 0.5
164	2007N	PGC 43319	0.9 ± 1.8	0.0129	34.10 ± 0.20	N	T16	72	10.4 ± 0.2	11.8 ± 0.5
165	2007nq	UGC 595	-4.4 ± 1.2	0.0443	36.20 ± 0.19	F	T16	24	11.1 ± 0.3	13.3 ± 1.1
166	2007O	UGC 9612	4.9 ± 0.5	0.0362	35.80 ± 0.17	N	T16	8	10.9 ± 0.2	12.8 ± 0.7
167	2007on	NGC 1404	-4.8 ± 0.5	0.0063	31.40 ± 0.22	SFP	T16	44	10.9 ± 0.1	12.8 ± 0.7
168	2007S	UGC 5378	3.1 ± 0.5	0.0145	33.90 ± 0.17	N	T16	49	10.1 ± 0.1	11.6 ± 0.4
169	2007st	NGC 692	4.1 ± 0.7	0.0212	34.70 ± 0.18	M	M14	45	11.2 ± 0.1	13.6 ± 0.6
170	2008ae	IC 577	4.8 ± 1.8	0.0301	35.60 ± 0.12	M	M14	17	10.7 ± 0.1	12.3 ± 0.6
171	2008ar	IC 3284	1.8 ± 2.0	0.0261	35.30 ± 0.20	N	T16	35	10.4 ± 0.2	11.9 ± 0.5
172	2008bc	PGC 90108	3.0 ± 2.0	0.0157	33.90 ± 0.20	N	T16	43	10.1 ± 0.1	11.6 ± 0.4
173	2008bf	NGC 4055	-5.0 ± 0.5	0.0240	35.30 ± 0.03	M	M14	45	11.3 ± 0.2	13.7 ± 0.7
174	2008bi	NGC 2618	1.5 ± 0.6	0.0137	33.80 ± 0.28	M	M14	41	10.9 ± 0.2	12.8 ± 0.8
175	2008cc	PGC 66000	-4.0 ± 0.7	0.0104	32.00 ± 0.50	P	T16	46	10.2 ± 0.3	11.7 ± 0.5
176	2008fp	PGC 20551	-1.8 ± 0.9	0.0060	31.60 ± 0.75	M	M14	62	10.2 ± 0.4	11.7 ± 0.6
177	2008fu	PGC 11470	5.0 ± 3.0	0.0524	36.80 ± 0.07	M	M14	54	10.9 ± 0.2	12.8 ± 0.7
178	2008fw	NGC 3261	3.6 ± 0.9	0.0084	32.70 ± 0.46	M	M14	41	10.9 ± 0.3	12.7 ± 0.9
179	2008gl	UGC 881	-4.8 ± 0.6	0.0340	35.60 ± 0.20	N	T16	64	11.0 ± 0.2	13.1 ± 0.7
180	2008gp	PGC 12669	1.5 ± 1.9	0.0328	35.60 ± 0.20	N	T16	38	10.9 ± 0.2	12.7 ± 0.7
181	2008ha	UGC 12682	9.8 ± 0.5	0.0046	31.70 ± 0.74	M	M14	36	9.4 ± 0.4	11.2 ± 0.5
182	2008hj	PGC 282	1.3 ± 1.3	0.0379	36.00 ± 0.20	N	T16	38	10.5 ± 0.2	11.9 ± 0.5
183	2008J	PGC 9800	3.9 ± 0.6	0.0159	34.10 ± 0.30	HI	T16	70	10.7 ± 0.2	12.2 ± 0.7
184	2008L	NGC 1259	-3.0 ± 2.0	0.0193	34.20 ± 0.17	N	T16	57	10.6 ± 0.1	12.1 ± 0.5
185	2008R	NGC 1200	-2.9 ± 0.6	0.0129	33.50 ± 0.19	P	T16	64	11.1 ± 0.1	13.2 ± 0.6
186	2008s1	UGC 8472	-1.9 ± 0.6	0.0221	35.20 ± 0.14	M	M14	69	10.9 ± 0.1	12.7 ± 0.7
187	2009al	NGC 3425	-2.0 ± 0.4	0.0231	34.90 ± 0.20	N	T16	34	10.8 ± 0.1	12.6 ± 0.6
188	2009an	NGC 4332	1.1 ± 0.5	0.0092	33.20 ± 0.36	M	M14	41	10.7 ± 0.2	12.3 ± 0.7
189	2009cz	NGC 2789	-0.2 ± 0.8	0.0211	34.90 ± 0.17	M	M14	31	11.1 ± 0.1	13.2 ± 0.6
190	2009D	PGC 14075	3.2 ± 1.3	0.0250	35.00 ± 0.18	H	T16	63	10.6 ± 0.1	12.0 ± 0.5
191	2009dc	UGC 10064	-1.8 ± 1.1	0.0216	34.90 ± 0.16	M	M14	79	10.8 ± 0.1	12.5 ± 0.6

Continued on next page

Table E1 – *Continued from previous page*

ID	SN name	host name	Hubble type	z	μ [mag]	method	ref	i [°]	$\log_{10}(M_*)$ [dex(M$_\odot$)]	$\log_{10}(M_{200})$ [dex(M$_\odot$)]
192	2009ds	NGC 3905	4.7 ± 0.5	0.0192	34.70 ± 0.20	N	T16	48	11.0 ± 0.2	12.9 ± 0.7
193	2009F	NGC 1725	−2.6 ± 0.6	0.0129	33.60 ± 0.30	M	M14	25	10.8 ± 0.2	12.5 ± 0.7
194	2009fv	NGC 6173	−4.8 ± 0.5	0.0293	34.90 ± 0.44	F	T16	77	11.3 ± 0.2	13.8 ± 0.9
195	2009I	NGC 1080	4.7 ± 0.5	0.0262	35.30 ± 0.14	M	M14	33	10.8 ± 0.1	12.6 ± 0.6
196	2009ig	NGC 1015	1.0 ± 0.4	0.0086	32.50 ± 0.08	C	R16	2	10.4 ± 0.2	11.8 ± 0.5
197	2009le	PGC 8223	4.2 ± 0.7	0.0178	34.20 ± 0.18	H	T16	57	10.9 ± 0.1	12.8 ± 0.6
198	2009Y	NGC 5728	1.2 ± 0.7	0.0093	32.90 ± 0.18	I	T16	53	11.0 ± 0.1	12.9 ± 0.6
199	2010B	NGC 5370	−1.8 ± 0.7	0.0102	33.40 ± 0.33	M	M14	16	10.4 ± 0.2	11.9 ± 0.5
200	2010kg	NGC 1633	2.1 ± 0.7	0.0166	34.20 ± 0.22	M	M14	36	10.7 ± 0.1	12.2 ± 0.6
201	2011by	NGC 3972	4.0 ± 0.3	0.0028	31.60 ± 0.07	C	R16	76	9.9 ± 0.1	11.4 ± 0.3
202	2011de	UGC 10018	3.6 ± 0.6	0.0292	35.60 ± 0.12	M	M14	15	10.9 ± 0.1	12.8 ± 0.7
203	2011fe	NGC 5457	5.9 ± 0.3	0.0008	29.10 ± 0.05	C	R16	16	10.5 ± 0.1	11.9 ± 0.5
204	2011hb	NGC 7674	3.8 ± 0.6	0.0289	35.50 ± 0.12	M	M14	18	11.4 ± 0.1	14.0 ± 0.6
205	2011im	NGC 7364	0.2 ± 1.1	0.0162	34.20 ± 0.40	H	T16	52	11.0 ± 0.2	12.9 ± 0.8
206	2012cg	NGC 4424	1.3 ± 1.6	0.0015	31.10 ± 0.29	C	R16	64	9.9 ± 0.2	11.4 ± 0.4
207	2012dn	PGC 64605	5.9 ± 0.5	0.0102	33.00 ± 0.40	H	T16	45	10.0 ± 0.3	11.5 ± 0.5
208	2012fr	NGC 1365	3.2 ± 0.7	0.0054	31.30 ± 0.06	C	R16	59	11.0 ± 0.1	13.2 ± 0.6
209	2012hr	PGC 18880	3.9 ± 0.5	0.0080	33.00 ± 0.40	H	T16	43	10.7 ± 0.2	12.3 ± 0.7
210	2012ht	NGC 3447	8.8 ± 0.6	0.0036	31.90 ± 0.04	C	R16	55	8.8 ± 0.1	10.9 ± 0.3
211	2012Z	NGC 1309	3.9 ± 0.6	0.0071	32.50 ± 0.14	CN	T16	9	10.4 ± 0.1	11.9 ± 0.4
212	2013aa	NGC 5643	5.0 ± 0.3	0.0040	31.00 ± 1.01	M	M14	27	10.6 ± 0.5	12.2 ± 1.1
213	2013cv	PGC 5068206	9.5 ± 1.5	0.0350	36.00 ± 1.00	M	M14	20	9.1 ± 0.9	11.0 ± 0.7
214	2013dy	NGC 7250	7.2 ± 2.0	0.0039	31.50 ± 0.08	C	R16	79	9.6 ± 0.1	11.3 ± 0.4
215	2013gs	UGC 5066	4.1 ± 0.5	0.0169	34.40 ± 0.21	M	M14	69	9.9 ± 0.2	11.4 ± 0.4
216	2013gy	NGC 1418	3.1 ± 0.7	0.0140	33.30 ± 0.40	H	T16	57	10.1 ± 0.2	11.6 ± 0.5
217	2013Q	NGC 7753	3.8 ± 0.6	0.0172	34.40 ± 0.21	M	M14	32	11.4 ± 0.1	14.1 ± 0.7
218	2014dg	UGC 2855	5.0 ± 0.5	0.0040	30.80 ± 0.40	H	T16	66	10.5 ± 0.2	12.0 ± 0.6
219	2015F	NGC 2442	3.7 ± 0.6	0.0054	31.50 ± 0.05	C	R16	30	10.9 ± 0.1	12.9 ± 0.5
220	2016bln	NGC 5221	2.9 ± 0.5	0.0233	35.10 ± 0.15	M	M14	62	11.1 ± 0.1	13.3 ± 0.6
221	2016dwu	PGC 11768	7.0 ± 0.4	0.0149	33.90 ± 0.26	M	M14	34	9.8 ± 0.5	11.4 ± 0.6
222	2018oh	UGC 4780	8.0 ± 0.5	0.0110	33.40 ± 0.33	M	M14	39	9.5 ± 0.4	11.2 ± 0.5
223	LSQ12gdj	PGC 72841	4.6 ± 2.2	0.0300	35.10 ± 0.20	N	T16	38	9.6 ± 0.2	11.3 ± 0.4
224	PTF11kx	PGC 3131180	4.3 ± 2.6	0.0466	36.60 ± 0.08	M	M14	65	10.2 ± 0.1	11.6 ± 0.4

Table E1: List of host galaxies used in the analysis. z = redshift (the error δz is globally neglected); μ = distance modulus; method for distance modulus determination: C = cepheid, T = tip of RGB from HST, L = tip of RGB from literature, M = miscellaneous, S = surface brightness fluctuation, N = SN Ia, H = Tully-Fisher relation with optical photometry, I = Tully-Fisher relation with 3.6 Spitzer, F = fundamental plane from CF2, P = fundamental plane from 6dFDS; reference for the distance modulus: T16 = Tully et al. (2016) (cosmicflows-3), R16 = Riess et al. (2016), M14 = Makarov et al. (2014) (HyperLEDA: http://leda.univ-lyon1.fr/); i = inclination of galactic disk (0° = face-on, 90° = edge-on) from HyperLEDA (error estimation globally $\delta i = 2°$); M_* = stellar mass; M_{200} = halo mass.

Table E2: Local SN information

ID	SN name	Ia-type	$\Delta m_{15}(B)$ [mag]	ref	$M_{\rm wd}$ [M$_\odot$]	θ ["]	$r_\perp$ [kpc]	ϕ [°]	r [kpc]	$\log_{10}(\rho_\chi)$ [dex(M$_\odot$ Mpc^{-3})]	v_χ [100 km s^{-1}]
1	1885A	N	2.20 ± 0.25	T17	0.49 ± 0.16	14.5	0.05 ± 0.0	35	0.1 ± 0.0	17.9 ± 0.2	0.6 ± 0.1
2	1939A	N	1.20 ± 0.80	TOSC	1.20 ± 0.90	22.1	1.61 ± 0.3	24	2.1 ± 0.5	16.8 ± 0.3	2.0 ± 0.8
3	1939B	N	2.00 ± 0.80	TOSC	0.60 ± 0.34	57.3	4.24 ± 0.5	18	5.8 ± 1.5	16.2 ± 0.4	2.3 ± 0.9
4	1980N	N	1.18 ± 0.16	TOSC	1.22 ± 0.27	210.0	17.56 ± 1.3	43	31.1 ± 6.0	15.7 ± 0.3	6.8 ± 2.6
5	1981B	N	1.14 ± 0.06	B18a	1.27 ± 0.17	55.8	4.05 ± 0.2	88	18.0 ± 4.9	15.2 ± 0.5	1.7 ± 0.6
6	1981D	N	1.15 ± 0.26	TOSC	1.26 ± 0.38	97.9	8.19 ± 0.6	38	13.6 ± 2.6	16.2 ± 0.3	5.7 ± 2.0
7	1986A	N	1.20 ± 0.80	TOSC	1.20 ± 0.90	22.8	4.90 ± 1.0	82	7.3 ± 1.9	16.2 ± 0.4	2.8 ± 1.3
8	1986G	91bg	1.70 ± 0.12	TOSC	0.78 ± 0.16	104.0	1.84 ± 0.1	5	1.9 ± 0.2	16.7 ± 0.2	1.5 ± 0.5
9	1989A	N	1.22 ± 0.30	TOSC	1.18 ± 0.39	32.8	6.06 ± 1.3	45	6.4 ± 1.5	15.9 ± 0.4	1.6 ± 0.6
10	1989B	N	1.60 ± 0.40	TOSC	0.86 ± 0.31	51.8	2.25 ± 0.2	32	3.1 ± 0.5	16.5 ± 0.2	1.7 ± 0.5
11	1990N	N	0.96 ± 0.06	B18a	1.48 ± 0.19	61.3	5.98 ± 0.3	39	7.4 ± 0.7	15.7 ± 0.2	1.4 ± 0.4
12	1991bg	91bg	1.63 ± 0.10	TOSC	0.83 ± 0.15	57.6	4.67 ± 0.4	48	5.1 ± 0.6	16.4 ± 0.2	3.2 ± 1.0
13	1991T	91T	0.78 ± 0.08	TOSC	1.74 ± 0.28	51.4	3.29 ± 0.3	43	12.0 ± 4.7	15.6 ± 0.5	2.0 ± 0.7

Continued on next page

Table E2 – *Continued from previous page*

ID	SN name	Ia-type	$\Delta m_{15}(B)$ [mag]	ref	$M_{\rm wd}$ [$M_\odot$]	θ ["]	$r_\perp$ [kpc]	ϕ [°]	r [kpc]	$\log_{10}(\rho_\chi)$ [dex($M_\odot\,{\rm Mpc}^{-3}$)]	v_χ [$100\,{\rm km\,s}^{-1}$]
14	1992al	N	1.06 ± 0.12	TOSC	1.36 ± 0.25	20.8	5.48 ± 0.7	29	14.7 ± 6.2	15.2 ± 0.6	1.5 ± 0.5
15	1992bo	N	1.56 ± 0.04	TOSC	0.88 ± 0.12	74.3	27.22 ± 2.5	34	37.9 ± 6.6	14.6 ± 0.5	1.9 ± 0.8
16	1993H	N	1.46 ± 0.40	TOSC	0.96 ± 0.36	13.2	5.68 ± 0.9	27	5.7 ± 0.9	16.2 ± 0.3	2.2 ± 0.9
17	1994ae	N	0.92 ± 0.06	B18a	1.54 ± 0.20	31.2	3.89 ± 0.2	45	7.8 ± 1.5	15.7 ± 0.3	1.4 ± 0.3
18	1994S	N	0.85 ± 0.24	TOSC	1.63 ± 0.56	16.0	4.74 ± 0.7	88	13.2 ± 3.7	15.6 ± 0.4	2.1 ± 0.8
19	1995ak	N	1.76 ± 0.20	TOSC	0.74 ± 0.18	8.0	2.87 ± 0.6	16	3.5 ± 1.0	16.3 ± 0.3	1.4 ± 0.4
20	1995al	N	0.89 ± 0.06	B18a	1.57 ± 0.21	16.0	2.42 ± 0.3	50	4.0 ± 0.8	16.2 ± 0.2	1.5 ± 0.4
21	1995bd	N	0.89 ± 0.12	TOSC	1.58 ± 0.31	23.2	5.90 ± 0.7	4	6.1 ± 1.0	16.0 ± 0.3	1.9 ± 0.6
22	1995D	N	1.01 ± 0.08	TOSC	1.42 ± 0.21	91.6	13.62 ± 1.4	18	14.5 ± 1.9	15.5 ± 0.4	2.1 ± 0.8
23	1995E	N	1.18 ± 0.12	TOSC	1.22 ± 0.22	22.9	4.84 ± 0.6	25	4.8 ± 0.6	16.1 ± 0.2	1.6 ± 0.5
24	1996bl	N	1.19 ± 0.20	TOSC	1.21 ± 0.30	5.9	3.70 ± 0.9	13	3.7 ± 0.9	16.3 ± 0.3	1.6 ± 0.5
25	1996bo	N	1.22 ± 0.08	TOSC	1.18 ± 0.18	5.2	1.45 ± 0.4	75	2.1 ± 0.7	16.7 ± 0.3	1.9 ± 0.7
26	1997bp	N	1.22 ± 0.08	TOSC	1.18 ± 0.18	24.0	3.44 ± 0.4	7	3.5 ± 0.4	16.2 ± 0.2	1.3 ± 0.3
27	1997bq	N	1.03 ± 0.16	TOSC	1.39 ± 0.32	78.5	14.65 ± 1.3	23	14.8 ± 1.4	16.1 ± 0.2	5.6 ± 1.9
28	1997do	N	1.16 ± 0.20	TOSC	1.24 ± 0.31	3.0	0.60 ± 0.2	80	0.8 ± 0.4	16.9 ± 0.3	0.9 ± 0.3
29	1997E	N	1.50 ± 0.16	TOSC	0.93 ± 0.20	64.9	17.37 ± 1.6	10	17.6 ± 1.8	16.0 ± 0.2	5.9 ± 2.1
30	1998ab	91T	1.13 ± 0.40	TOSC	1.28 ± 0.55	15.1	6.46 ± 0.9	24	6.5 ± 0.9	16.1 ± 0.3	2.2 ± 0.8
31	1998aq	N	1.05 ± 0.06	B18a	1.37 ± 0.18	20.7	2.22 ± 0.2	88	2.4 ± 0.2	16.4 ± 0.2	1.3 ± 0.3
32	1998bp	N	1.77 ± 0.08	TOSC	0.73 ± 0.13	12.9	2.47 ± 0.4	72	5.6 ± 1.5	16.0 ± 0.3	1.7 ± 0.5
33	1998bu	N	0.90 ± 0.26	TOSC	1.57 ± 0.55	55.6	2.86 ± 0.2	15	3.0 ± 0.3	16.4 ± 0.2	1.7 ± 0.5
34	1998de	91bg	1.80 ± 0.12	TOSC	0.72 ± 0.15	72.2	22.37 ± 2.1	42	24.7 ± 2.9	15.6 ± 0.3	4.6 ± 1.8
35	1998dh	N	1.17 ± 0.06	TOSC	1.23 ± 0.16	54.5	8.25 ± 0.7	18	11.4 ± 2.5	15.8 ± 0.4	2.5 ± 0.9
36	1998ef	N	1.24 ± 0.08	TOSC	1.16 ± 0.17	7.3	2.04 ± 0.4	3	2.1 ± 0.5	16.6 ± 0.2	1.4 ± 0.4
37	1998es	91T	0.81 ± 0.12	TOSC	1.69 ± 0.35	11.9	2.08 ± 0.3	37	2.2 ± 0.4	16.5 ± 0.2	1.2 ± 0.3
38	1999aa	91T	0.72 ± 0.04	TOSC	1.83 ± 0.20	30.2	9.14 ± 1.0	39	9.4 ± 1.2	16.0 ± 0.3	2.7 ± 1.2
39	1999ac	pec	1.19 ± 0.14	TOSC	1.21 ± 0.24	39.7	7.68 ± 0.7	29	8.3 ± 1.0	15.6 ± 0.3	1.4 ± 0.4
40	1999bh	02es	1.33 ± 0.11	T17	1.08 ± 0.19	10.3	4.70 ± 1.3	44	6.5 ± 2.3	16.1 ± 0.5	2.3 ± 1.2
41	1999by	91bg	1.80 ± 0.04	TOSC	0.72 ± 0.12	134.4	9.47 ± 0.7	17	11.7 ± 1.9	16.0 ± 0.3	3.5 ± 1.3
42	1999cc	N	1.59 ± 0.14	TOSC	0.86 ± 0.18	17.4	10.19 ± 1.4	36	11.5 ± 2.0	16.1 ± 0.3	4.7 ± 1.8
43	1999cl	N	1.18 ± 0.06	TOSC	1.22 ± 0.16	54.4	5.18 ± 0.8	28	6.9 ± 1.7	16.4 ± 0.3	4.0 ± 1.7
44	1999cp	N	0.99 ± 0.03	TOSC	1.44 ± 0.14	59.4	12.28 ± 1.2	10	12.3 ± 1.2	15.4 ± 0.3	1.5 ± 0.5
45	1999dk	N	1.42 ± 0.10	TOSC	0.99 ± 0.17	27.4	7.60 ± 0.8	79	7.8 ± 1.0	15.7 ± 0.3	1.4 ± 0.4
46	1999dq	91T	0.89 ± 0.08	TOSC	1.58 ± 0.24	7.7	1.68 ± 0.3	80	1.8 ± 0.4	16.8 ± 0.2	1.7 ± 0.6
47	1999ee	N	0.93 ± 0.04	TOSC	1.52 ± 0.17	11.9	2.39 ± 0.4	72	6.4 ± 1.9	16.2 ± 0.3	2.7 ± 1.0
48	1999ej	N	1.53 ± 0.06	TOSC	0.91 ± 0.14	21.7	6.78 ± 0.8	28	7.4 ± 1.1	16.0 ± 0.3	2.3 ± 0.8
49	1999ek	N	1.19 ± 0.06	TOSC	1.21 ± 0.16	15.7	4.92 ± 0.7	42	11.3 ± 3.5	15.8 ± 0.4	2.7 ± 1.1
50	1999gh	N	2.00 ± 0.60	TOSC	0.60 ± 0.28	54.1	7.94 ± 0.8	33	9.7 ± 1.4	16.1 ± 0.3	3.4 ± 1.3
51	2000cn	N	1.53 ± 0.08	TOSC	0.91 ± 0.15	11.8	5.21 ± 0.8	16	5.2 ± 0.9	16.4 ± 0.3	2.9 ± 1.1
52	2000cw	N	1.25 ± 0.06	TOSC	1.15 ± 0.16	22.4	10.84 ± 2.0	28	14.7 ± 4.0	15.5 ± 0.5	2.3 ± 1.1
53	2000cx	91T	0.97 ± 0.04	TOSC	1.47 ± 0.16	110.8	12.69 ± 1.8	10	12.7 ± 1.8	15.9 ± 0.3	3.5 ± 1.5
54	2000E	N	0.90 ± 0.20	TOSC	1.56 ± 0.45	30.5	2.75 ± 0.3	16	2.8 ± 0.4	16.5 ± 0.2	1.8 ± 0.7
55	2001ah	pec	0.72 ± 0.18	TOSC	1.83 ± 0.56	32.9	33.26 ± 3.6	48	34.3 ± 4.2	15.4 ± 0.5	4.6 ± 2.6
56	2001ba	N	1.01 ± 0.04	TOSC	1.42 ± 0.16	26.8	15.39 ± 1.7	42	15.8 ± 1.9	15.9 ± 0.3	4.1 ± 1.5
57	2001bt	N	1.32 ± 0.08	TOSC	1.09 ± 0.17	21.4	5.03 ± 0.6	59	5.7 ± 0.8	16.3 ± 0.2	2.7 ± 0.9
58	2001cj	N	0.92 ± 0.08	TOSC	1.54 ± 0.23	34.5	19.10 ± 0.8	81	19.5 ± 1.0	15.3 ± 0.3	2.2 ± 0.7
59	2001cz	N	1.01 ± 0.06	TOSC	1.42 ± 0.18	33.0	8.88 ± 0.9	12	11.2 ± 2.7	15.9 ± 0.4	2.8 ± 1.1
60	2001da	N	1.20 ± 0.06	TOSC	1.20 ± 0.16	11.3	3.51 ± 0.6	89	10.8 ± 3.4	15.6 ± 0.5	1.9 ± 0.7
61	2001dl	N	1.00 ± 0.06	TOSC	1.43 ± 0.19	11.1	5.94 ± 1.2	28	14.4 ± 6.8	15.5 ± 0.6	2.0 ± 0.9
62	2001eh	N	0.74 ± 0.04	TOSC	1.80 ± 0.20	38.0	25.23 ± 2.6	15	25.3 ± 2.7	15.6 ± 0.4	4.8 ± 2.3
63	2001ep	N	1.42 ± 0.06	TOSC	0.99 ± 0.14	18.6	4.41 ± 0.6	5	4.4 ± 0.6	16.1 ± 0.2	1.4 ± 0.4
64	2001gb	N	1.40 ± 1.00	TOSC	1.01 ± 0.82	15.1	7.64 ± 1.1	83	7.8 ± 1.2	16.0 ± 0.3	2.4 ± 0.9
65	2002bf	N	1.30 ± 1.00	TOSC	1.10 ± 0.95	4.0	1.73 ± 0.6	34	2.0 ± 0.7	16.7 ± 0.3	1.6 ± 0.6
66	2002bo	N	1.10 ± 0.04	TOSC	1.31 ± 0.15	16.0	1.71 ± 0.2	25	2.9 ± 0.9	16.6 ± 0.3	2.0 ± 0.7
67	2002cd	N	0.90 ± 0.06	TOSC	1.56 ± 0.20	12.9	2.70 ± 0.4	40	3.5 ± 0.8	16.4 ± 0.3	1.8 ± 0.6
68	2002cf	91bg	1.87 ± 0.14	TOSC	0.67 ± 0.15	20.0	5.17 ± 1.5	44	7.3 ± 2.6	16.3 ± 0.5	3.6 ± 2.0
69	2002cr	N	1.21 ± 0.06	TOSC	1.19 ± 0.16	64.2	13.27 ± 1.2	20	13.3 ± 1.3	15.3 ± 0.3	1.5 ± 0.5
70	2002cs	N	1.00 ± 0.06	TOSC	1.43 ± 0.19	25.3	6.18 ± 1.0	25	6.6 ± 1.3	16.2 ± 0.3	2.6 ± 1.1
71	2002cx	02cx	1.26 ± 0.20	TOSC	1.14 ± 0.28	15.2	11.50 ± 0.9	4	12.2 ± 2.1	15.3 ± 0.4	1.4 ± 0.4
72	2002de	N	1.07 ± 0.04	TOSC	1.34 ± 0.15	2.3	1.22 ± 0.6	78	1.6 ± 0.9	16.9 ± 0.4	2.0 ± 0.9
73	2002do	N	1.75 ± 0.24	TOSC	0.75 ± 0.20	8.8	2.76 ± 0.5	37	3.2 ± 0.7	16.7 ± 0.3	2.9 ± 1.0
74	2002dp	N	1.40 ± 0.10	TOSC	1.01 ± 0.17	37.1	7.82 ± 0.8	30	8.1 ± 0.9	16.0 ± 0.3	2.3 ± 0.8
75	2002eb	N	0.88 ± 0.08	TOSC	1.59 ± 0.24	19.5	11.36 ± 0.8	60	13.7 ± 1.5	15.6 ± 0.3	2.3 ± 0.7
76	2002ef	N	1.18 ± 0.14	TOSC	1.23 ± 0.25	10.9	2.73 ± 0.9	9	2.7 ± 0.9	16.5 ± 0.4	1.8 ± 0.9
77	2002el	N	1.27 ± 0.08	TOSC	1.13 ± 0.17	27.3	14.80 ± 0.8	29	20.0 ± 2.9	15.8 ± 0.2	5.0 ± 1.5

Continued on next page

Table E2 – *Continued from previous page*

ID	SN name	Ia-type	$\Delta m_{15}(B)$ [mag]	ref	$M_{\rm wd}$ [$M_\odot$]	θ ["]	$r_\perp$ [kpc]	ϕ [°]	r [kpc]	$\log_{10}(\rho_\chi)$ [dex($M_\odot$ Mpc^{-3})]	v_χ [100 km s^{-1}]
78	2002er	N	1.26 ± 0.08	TOSC	1.14 ± 0.17	11.2	1.63 ± 0.3	9	1.8 ± 0.5	16.5 ± 0.2	1.1 ± 0.3
79	2002es	02es	1.28 ± 0.08	TOSC	1.12 ± 0.17	32.0	11.70 ± 1.3	70	11.9 ± 1.4	16.1 ± 0.4	4.4 ± 2.7
80	2002fb	91bg	1.86 ± 0.18	TOSC	0.68 ± 0.17	20.5	6.29 ± 0.8	33	6.5 ± 0.9	16.3 ± 0.2	3.4 ± 1.1
81	2002fk	N	1.04 ± 0.08	B18a	1.38 ± 0.20	12.7	1.94 ± 0.2	12	1.9 ± 0.2	16.6 ± 0.2	1.4 ± 0.3
82	2002G	N	1.43 ± 0.05	B18b	0.99 ± 0.13	8.8	5.70 ± 1.1	60	6.8 ± 1.6	16.2 ± 0.3	3.1 ± 1.2
83	2002ha	N	1.42 ± 0.12	TOSC	1.00 ± 0.18	30.2	8.20 ± 0.8	45	9.7 ± 1.4	16.2 ± 0.2	3.9 ± 1.3
84	2002hw	N	1.34 ± 0.80	TOSC	1.07 ± 0.74	8.8	2.93 ± 0.6	29	3.0 ± 0.6	16.5 ± 0.3	1.7 ± 0.6
85	2002ic	CSM	0.39 ± 0.17	T17	2.33 ± 1.11	4.0	4.81 ± 1.6	10	5.0 ± 1.8	15.8 ± 0.6	1.0 ± 0.5
86	2002jy	N	0.77 ± 0.20	TOSC	1.75 ± 0.55	59.5	23.92 ± 2.2	1	23.9 ± 2.2	15.3 ± 0.5	2.8 ± 1.5
87	2003cg	N	1.19 ± 0.04	TOSC	1.21 ± 0.14	19.8	2.21 ± 0.3	31	2.4 ± 0.4	16.7 ± 0.2	2.2 ± 0.7
88	2003cq	N	1.26 ± 0.24	TOSC	1.14 ± 0.32	28.8	17.94 ± 2.0	1	17.9 ± 2.0	16.0 ± 0.3	6.5 ± 2.4
89	2003du	N	0.98 ± 0.06	B18a	1.46 ± 0.19	16.4	3.01 ± 0.3	10	3.0 ± 0.3	16.1 ± 0.2	1.0 ± 0.2
90	2003fa	N	0.83 ± 0.04	TOSC	1.67 ± 0.18	51.0	37.49 ± 3.7	6	38.1 ± 4.3	15.1 ± 0.5	3.2 ± 1.6
91	2003gn	N	1.28 ± 0.06	TOSC	1.12 ± 0.15	18.7	14.56 ± 1.8	2	14.6 ± 2.0	15.7 ± 0.3	3.0 ± 1.2
92	2003gq	02cx	1.67 ± 0.20	TOSC	0.80 ± 0.20	14.9	7.40 ± 1.9	7	7.6 ± 2.1	16.2 ± 0.4	3.3 ± 1.8
93	2003he	N	1.01 ± 0.06	TOSC	1.42 ± 0.18	6.0	2.93 ± 1.0	20	4.4 ± 2.2	16.2 ± 0.5	1.7 ± 0.9
94	2003W	N	1.12 ± 0.06	TOSC	1.29 ± 0.17	4.2	1.56 ± 0.5	50	2.0 ± 0.7	16.7 ± 0.3	1.8 ± 0.7
95	2003Y	91bg	1.72 ± 0.06	TOSC	0.77 ± 0.13	20.0	6.41 ± 0.4	4	6.4 ± 0.5	16.1 ± 0.2	2.3 ± 0.6
96	2004at	N	1.17 ± 0.08	TOSC	1.23 ± 0.18	19.7	9.95 ± 0.6	9	10.7 ± 1.3	15.9 ± 0.4	2.9 ± 1.7
97	2004bg	N	0.95 ± 0.12	TOSC	1.49 ± 0.29	17.9	7.37 ± 1.0	3	7.8 ± 1.8	15.8 ± 0.4	1.8 ± 0.6
98	2004bk	N	1.05 ± 0.40	TOSC	1.37 ± 0.62	9.9	4.92 ± 0.6	42	4.9 ± 0.6	16.3 ± 0.2	2.1 ± 0.7
99	2004bw	N	1.28 ± 0.04	TOSC	1.12 ± 0.14	23.7	11.28 ± 1.0	75	12.8 ± 1.5	15.7 ± 0.4	2.5 ± 1.3
100	2004dt	N	1.10 ± 0.06	B18a	1.31 ± 0.17	12.5	4.63 ± 0.5	80	5.3 ± 0.7	16.3 ± 0.2	2.4 ± 0.7
101	2004ef	N	1.33 ± 0.06	B18a	1.08 ± 0.15	9.9	5.35 ± 1.0	50	5.3 ± 1.0	16.3 ± 0.3	2.5 ± 1.0
102	2004eo	N	1.31 ± 0.06	B18a	1.09 ± 0.15	59.8	16.50 ± 1.6	29	38.4 ± 13.1	15.4 ± 0.5	5.0 ± 2.2
103	2004ey	N	0.97 ± 0.06	B18a	1.47 ± 0.19	14.6	4.32 ± 0.6	3	4.3 ± 0.6	16.1 ± 0.2	1.3 ± 0.3
104	2004fz	N	1.45 ± 0.06	TOSC	0.97 ± 0.14	12.8	3.67 ± 0.4	43	4.3 ± 0.6	16.4 ± 0.2	2.2 ± 0.6
105	2004gs	N	1.56 ± 0.06	B18a	0.89 ± 0.13	16.3	9.16 ± 1.3	16	9.3 ± 1.4	16.0 ± 0.3	2.7 ± 1.0
106	2004L	N	1.60 ± 1.00	TOSC	0.86 ± 0.63	3.2	1.97 ± 0.8	1	2.0 ± 0.8	16.7 ± 0.4	1.5 ± 0.6
107	2005A	N	1.06 ± 0.06	B18a	1.36 ± 0.18	6.3	2.09 ± 0.5	75	6.2 ± 2.4	16.5 ± 0.3	4.4 ± 1.6
108	2005ag	N	0.92 ± 0.06	B18a	1.54 ± 0.20	9.2	12.33 ± 2.3	39	13.7 ± 3.0	16.0 ± 0.3	4.4 ± 1.8
109	2005al	N	1.34 ± 0.06	B18a	1.07 ± 0.15	18.6	5.55 ± 0.7	21	6.0 ± 0.9	16.2 ± 0.3	2.7 ± 0.9
110	2005am	N	1.49 ± 0.06	B18a	0.94 ± 0.14	35.7	4.76 ± 0.5	14	5.7 ± 1.1	16.2 ± 0.3	2.3 ± 0.8
111	2005bg	N	1.02 ± 0.08	B18a	1.40 ± 0.21	0.7	0.33 ± 0.5	85	0.3 ± 0.3	17.4 ± 0.7	0.8 ± 0.4
112	2005bo	N	1.29 ± 0.06	B18a	1.11 ± 0.15	13.9	3.76 ± 0.6	11	3.8 ± 0.6	16.3 ± 0.2	1.7 ± 0.5
113	2005cc	02cx	2.07 ± 0.10	TOSC	0.56 ± 0.13	4.7	0.80 ± 0.3	26	0.8 ± 0.3	17.1 ± 0.4	1.4 ± 0.7
114	2005de	N	1.23 ± 0.08	TOSC	1.17 ± 0.18	32.6	12.01 ± 0.6	5	12.6 ± 1.2	15.7 ± 0.3	2.3 ± 0.7
115	2005el	N	1.35 ± 0.06	B18a	1.06 ± 0.15	44.7	12.74 ± 1.3	14	13.0 ± 1.4	15.9 ± 0.3	3.4 ± 1.3
116	2005eq	N	0.81 ± 0.06	B18a	1.69 ± 0.22	29.8	16.12 ± 1.8	15	21.1 ± 5.2	15.5 ± 0.5	3.2 ± 1.6
117	2005gj	CSM	0.10 ± 0.09	T17	2.67 ± 2.51	0.5	0.70 ± 1.6	88	3.7 ± 3.3	15.9 ± 1.2	0.9 ± 0.6
118	2005hc	N	0.88 ± 0.06	B18a	1.60 ± 0.21	8.2	7.01 ± 1.4	35	8.5 ± 2.1	16.0 ± 0.4	2.7 ± 1.1
119	2005hk	02cx	1.43 ± 0.08	TOSC	0.99 ± 0.16	18.8	5.27 ± 1.0	51	11.0 ± 3.6	15.2 ± 0.5	1.1 ± 0.3
120	2005iq	N	1.28 ± 0.06	B18a	1.12 ± 0.15	18.9	12.55 ± 1.6	12	13.3 ± 2.2	15.6 ± 0.4	2.3 ± 1.0
121	2005ir	N	0.88 ± 0.07	B18a	1.58 ± 0.22	3.1	4.37 ± 1.8	19	4.5 ± 1.9	16.2 ± 0.5	1.8 ± 1.0
122	2005kc	N	1.18 ± 0.06	B18a	1.23 ± 0.16	11.9	3.33 ± 0.5	62	5.9 ± 1.5	16.4 ± 0.3	3.3 ± 1.2
123	2005ke	91bg	1.69 ± 0.06	B18a	0.79 ± 0.13	56.4	7.96 ± 1.2	3	8.0 ± 1.3	16.2 ± 0.3	3.1 ± 1.5
124	2005ki	N	1.36 ± 0.06	B18a	1.05 ± 0.15	71.0	27.04 ± 2.5	42	29.3 ± 3.4	15.6 ± 0.3	5.1 ± 2.1
125	2005M	91T	0.80 ± 0.06	B18a	1.71 ± 0.23	9.8	4.59 ± 0.8	85	9.2 ± 2.5	15.6 ± 0.4	1.5 ± 0.5
126	2005mc	N	1.61 ± 0.07	B18a	0.85 ± 0.14	4.5	2.26 ± 0.7	46	2.3 ± 0.7	16.7 ± 0.3	2.2 ± 0.8
127	2005ms	N	0.75 ± 0.16	TOSC	1.78 ± 0.48	43.9	22.61 ± 2.3	78	22.8 ± 2.5	15.2 ± 0.4	2.2 ± 1.0
128	2005na	N	1.03 ± 0.06	B18a	1.39 ± 0.18	7.1	3.50 ± 0.8	74	5.4 ± 1.6	16.5 ± 0.3	3.4 ± 1.3
129	2005W	N	1.11 ± 0.06	B18a	1.30 ± 0.17	55.4	10.13 ± 1.6	15	10.6 ± 1.9	15.8 ± 0.4	2.4 ± 1.2
130	2006ac	N	1.50 ± 0.14	TOSC	0.93 ± 0.19	21.6	9.37 ± 1.2	70	9.4 ± 1.2	16.2 ± 0.2	3.8 ± 1.3
131	2006ax	N	0.99 ± 0.06	B18a	1.45 ± 0.19	54.2	18.01 ± 1.7	6	18.0 ± 1.7	15.5 ± 0.4	2.8 ± 1.3
132	2006az	N	1.21 ± 0.10	TOSC	1.20 ± 0.20	7.3	4.18 ± 0.9	3	4.2 ± 0.9	16.7 ± 0.2	4.1 ± 1.4
133	2006bh	N	1.39 ± 0.06	B18a	1.02 ± 0.14	52.9	11.48 ± 1.0	52	14.1 ± 1.9	15.7 ± 0.3	2.9 ± 1.1
134	2006bq	N	1.64 ± 0.16	TOSC	0.83 ± 0.18	3.3	1.36 ± 0.5	14	1.4 ± 0.6	16.9 ± 0.3	1.8 ± 0.7
135	2006br	N	1.11 ± 0.09	B18a	1.30 ± 0.21	5.5	3.17 ± 0.8	21	5.1 ± 2.2	16.5 ± 0.4	3.7 ± 1.6
136	2006bt	02es	1.08 ± 0.08	TOSC	1.33 ± 0.20	50.0	30.25 ± 3.0	32	31.4 ± 3.5	15.5 ± 0.4	4.6 ± 2.0
137	2006cp	N	1.13 ± 0.20	TOSC	1.28 ± 0.33	25.3	10.38 ± 1.2	60	10.7 ± 1.4	15.4 ± 0.3	1.4 ± 0.4
138	2006D	N	1.38 ± 0.06	B18a	1.04 ± 0.15	13.4	2.34 ± 0.4	4	2.3 ± 0.4	16.4 ± 0.2	1.2 ± 0.3
139	2006ef	N	1.36 ± 0.07	B18a	1.05 ± 0.16	26.2	9.21 ± 1.1	23	9.9 ± 1.4	15.7 ± 0.3	2.0 ± 0.7
140	2006em	91bg	1.65 ± 0.40	TOSC	0.82 ± 0.30	54.8	20.23 ± 4.7	45	57.1 ± 25.4	14.8 ± 0.9	3.6 ± 2.6
141	2006en	N	1.32 ± 0.16	TOSC	1.09 ± 0.23	5.2	3.18 ± 0.9	36	3.2 ± 0.9	16.7 ± 0.3	2.8 ± 1.0

Continued on next page

Table E2 – *Continued from previous page*

ID	SN name	Ia-type	$\Delta m_{15}(B)$ [mag]	ref	$M_{\rm wd}$ [$\mathrm{M_\odot}$]	θ ["]	$r_\perp$ [kpc]	ϕ [°]	r [kpc]	$\log_{10}(\rho_\chi)$ [dex($\mathrm{M_\odot\,Mpc^{-3}}$)]	v_χ [$100\,\mathrm{km\,s^{-1}}$]
142	2006et	N	0.89 ± 0.06	B18a	1.58 ± 0.21	10.7	4.19 ± 0.7	47	5.3 ± 1.2	16.4 ± 0.3	2.9 ± 1.1
143	2006gr	N	0.78 ± 0.06	TOSC	1.74 ± 0.23	34.7	22.92 ± 2.5	4	23.0 ± 2.5	16.1 ± 0.3	8.9 ± 4.1
144	2006gz	03fg	0.75 ± 0.12	TOSC	1.78 ± 0.39	28.5	16.55 ± 1.5	15	17.2 ± 1.9	15.3 ± 0.4	1.9 ± 0.8
145	2006hb	91bg	1.58 ± 0.07	B18a	0.87 ± 0.14	20.0	5.24 ± 0.7	27	6.2 ± 1.1	16.0 ± 0.3	1.7 ± 0.5
146	2006mr	pec	1.90 ± 0.06	B18a	0.65 ± 0.12	9.9	0.83 ± 0.1	18	1.0 ± 0.2	17.4 ± 0.2	2.5 ± 0.8
147	2006ob	N	1.51 ± 0.06	B18a	0.92 ± 0.14	6.5	6.80 ± 1.6	70	9.2 ± 2.6	16.3 ± 0.3	5.0 ± 2.0
148	2006ot	pec	1.05 ± 0.10	TOSC	1.37 ± 0.23	6.4	5.90 ± 1.3	40	10.0 ± 3.5	16.3 ± 0.4	5.6 ± 2.4
149	2006S	N	0.98 ± 0.10	TOSC	1.46 ± 0.25	11.6	7.52 ± 1.2	60	18.6 ± 5.8	15.3 ± 0.5	2.1 ± 0.9
150	2006X	N	1.06 ± 0.06	B18a	1.36 ± 0.18	48.8	3.26 ± 0.2	48	3.4 ± 0.3	16.4 ± 0.2	1.9 ± 0.7
151	2007A	N	0.95 ± 0.06	B18a	1.49 ± 0.20	10.3	3.19 ± 0.6	4	3.2 ± 0.6	16.4 ± 0.2	1.7 ± 0.5
152	2007af	N	1.08 ± 0.06	B18a	1.33 ± 0.17	46.0	5.02 ± 0.2	87	6.6 ± 0.6	15.5 ± 0.3	0.9 ± 0.3
153	2007ax	91bg	1.93 ± 0.06	B18a	0.64 ± 0.12	7.0	1.04 ± 0.4	52	3.0 ± 1.8	16.4 ± 0.5	1.5 ± 0.7
154	2007ba	91bg	1.69 ± 0.06	B18a	0.79 ± 0.13	13.1	11.15 ± 1.9	68	30.5 ± 9.8	15.7 ± 0.4	7.1 ± 3.2
155	2007bc	N	1.29 ± 0.06	B18a	1.11 ± 0.15	33.0	13.18 ± 1.4	34	13.5 ± 1.6	15.8 ± 0.3	3.0 ± 1.3
156	2007bd	N	1.27 ± 0.06	B18a	1.13 ± 0.15	9.8	5.72 ± 1.0	5	5.7 ± 1.0	16.3 ± 0.3	2.7 ± 1.1
157	2007bj	N	1.30 ± 0.40	TOSC	1.10 ± 0.44	4.7	1.87 ± 0.5	1	1.9 ± 0.5	16.9 ± 0.3	2.3 ± 0.8
158	2007bm	N	1.19 ± 0.06	B18a	1.21 ± 0.16	10.6	1.37 ± 0.2	5	1.4 ± 0.3	16.8 ± 0.2	1.4 ± 0.4
159	2007ci	N	1.85 ± 0.20	TOSC	0.69 ± 0.17	12.5	4.42 ± 0.7	29	4.6 ± 0.8	16.4 ± 0.3	2.7 ± 1.0
160	2007F	N	0.92 ± 0.06	TOSC	1.53 ± 0.20	12.0	5.66 ± 0.9	2	5.7 ± 0.9	15.9 ± 0.3	1.4 ± 0.4
161	2007hj	N	1.62 ± 0.06	B18a	0.84 ± 0.13	15.1	4.10 ± 0.4	25	4.3 ± 0.4	16.2 ± 0.2	1.7 ± 0.4
162	2007kk	N	1.18 ± 0.08	TOSC	1.23 ± 0.18	13.3	9.81 ± 1.6	23	10.1 ± 1.8	16.3 ± 0.3	5.1 ± 1.8
163	2007le	N	0.96 ± 0.06	B18a	1.48 ± 0.19	16.2	1.57 ± 0.3	6	1.9 ± 0.8	16.6 ± 0.3	1.2 ± 0.4
164	2007N	pec	1.89 ± 0.06	B18a	0.66 ± 0.12	16.1	5.03 ± 0.8	19	7.1 ± 2.1	15.8 ± 0.4	1.6 ± 0.6
165	2007nq	N	1.49 ± 0.06	B18a	0.94 ± 0.14	24.2	18.27 ± 2.4	20	18.5 ± 2.5	15.8 ± 0.5	4.4 ± 2.9
166	2007O	N	0.80 ± 0.40	TOSC	1.71 ± 0.95	10.0	6.52 ± 1.2	44	6.6 ± 1.2	16.2 ± 0.3	2.8 ± 1.1
167	2007on	N	1.67 ± 0.06	B18a	0.80 ± 0.13	70.3	6.33 ± 0.7	3	6.3 ± 0.7	16.2 ± 0.3	2.8 ± 1.0
168	2007S	N	0.80 ± 0.06	B18a	1.71 ± 0.23	11.7	3.31 ± 0.5	9	3.4 ± 0.6	16.2 ± 0.2	1.3 ± 0.3
169	2007st	N	1.43 ± 0.08	B18a	0.99 ± 0.16	5.3	2.16 ± 0.6	55	2.8 ± 0.9	16.8 ± 0.3	3.3 ± 1.2
170	2008ae	02cx	1.50 ± 0.12	TOSC	0.93 ± 0.17	13.2	7.95 ± 1.0	31	8.0 ± 1.1	15.9 ± 0.3	2.2 ± 0.8
171	2008ar	N	1.01 ± 0.06	B18a	1.42 ± 0.19	5.8	3.10 ± 0.8	20	3.2 ± 0.9	16.3 ± 0.3	1.5 ± 0.5
172	2008bc	N	0.89 ± 0.06	B18a	1.57 ± 0.21	19.6	5.52 ± 0.8	41	6.5 ± 1.2	15.8 ± 0.3	1.4 ± 0.4
173	2008bf	N	0.93 ± 0.06	B18a	1.53 ± 0.20	52.3	28.04 ± 0.9	25	30.4 ± 1.8	15.7 ± 0.3	6.1 ± 2.6
174	2008bi	N	1.98 ± 0.07	B18a	0.61 ± 0.12	4.6	1.24 ± 0.4	76	1.6 ± 0.6	16.9 ± 0.4	2.0 ± 1.0
175	2008cc	N	1.40 ± 0.07	B18a	1.01 ± 0.15	8.2	0.97 ± 0.3	57	1.3 ± 0.5	16.8 ± 0.3	1.1 ± 0.4
176	2008fp	N	0.81 ± 0.06	B18a	1.70 ± 0.23	18.5	1.88 ± 0.8	38	2.9 ± 1.4	16.3 ± 0.5	1.3 ± 0.6
177	2008fu	N	1.40 ± 0.07	B18a	1.01 ± 0.15	2.5	2.44 ± 1.1	19	2.7 ± 1.3	16.7 ± 0.4	2.3 ± 1.1
178	2008fw	N	0.84 ± 0.07	B18a	1.64 ± 0.24	66.8	10.84 ± 2.5	10	11.0 ± 2.6	15.9 ± 0.5	2.9 ± 1.7
179	2008gl	N	1.33 ± 0.06	B18a	1.08 ± 0.15	23.7	14.45 ± 1.9	13	15.9 ± 2.9	15.8 ± 0.4	4.0 ± 1.8
180	2008gp	N	1.02 ± 0.06	B18a	1.41 ± 0.18	17.4	10.29 ± 1.5	13	10.5 ± 1.6	15.9 ± 0.3	3.0 ± 1.3
181	2008ha	02cx	1.80 ± 0.40	TOSC	0.72 ± 0.26	9.4	0.99 ± 0.4	6	1.0 ± 0.5	16.8 ± 0.4	0.8 ± 0.3
182	2008hj	N	0.96 ± 0.06	B18a	1.48 ± 0.19	21.0	14.60 ± 2.0	68	18.0 ± 3.3	15.2 ± 0.5	1.8 ± 0.8
183	2008J	CSM	0.21 ± 0.09	T17	2.55 ± 1.19	4.8	1.51 ± 0.5	5	1.6 ± 0.6	16.8 ± 0.3	1.5 ± 0.6
184	2008L	N	1.04 ± 0.14	TOSC	1.38 ± 0.29	10.6	3.47 ± 0.6	61	5.8 ± 1.5	16.1 ± 0.3	1.8 ± 0.6
185	2008R	91bg	1.63 ± 0.06	B18a	0.83 ± 0.13	14.3	3.42 ± 0.5	20	4.2 ± 1.0	16.6 ± 0.3	3.1 ± 1.1
186	2008s1	N	1.35 ± 0.08	TOSC	1.06 ± 0.16	18.4	9.36 ± 1.1	10	10.3 ± 1.8	15.9 ± 0.3	2.9 ± 1.2
187	2009al	N	0.67 ± 0.06	B18a	1.90 ± 0.28	65.5	28.43 ± 3.1	74	33.9 ± 4.9	15.1 ± 0.5	2.9 ± 1.4
188	2009an	N	1.29 ± 0.06	TOSC	1.11 ± 0.15	26.8	5.60 ± 1.1	46	6.6 ± 1.6	16.0 ± 0.4	2.1 ± 0.9
189	2009cz	N	0.89 ± 0.06	B18a	1.57 ± 0.21	18.2	7.92 ± 1.1	40	8.5 ± 1.3	16.2 ± 0.3	3.7 ± 1.3
190	2009D	N	0.90 ± 0.06	B18a	1.57 ± 0.20	40.7	18.37 ± 2.0	62	36.7 ± 8.0	14.7 ± 0.6	1.9 ± 0.9
191	2009dc	03fg	0.73 ± 0.08	TOSC	1.81 ± 0.30	25.4	11.47 ± 1.3	46	44.0 ± 17.9	14.8 ± 0.7	2.8 ± 1.3
192	2009ds	N	0.80 ± 0.06	B18a	1.71 ± 0.24	12.6	4.99 ± 0.9	11	5.1 ± 0.9	16.4 ± 0.3	2.8 ± 1.2
193	2009F	pec	1.88 ± 0.06	B18a	0.67 ± 0.12	12.2	3.09 ± 0.7	28	3.2 ± 0.7	16.5 ± 0.3	2.0 ± 0.8
194	2009fv	N	1.80 ± 0.40	TOSC	0.72 ± 0.26	8.1	3.50 ± 1.1	52	12.4 ± 7.1	16.2 ± 0.6	5.3 ± 3.2
195	2009I	N	0.81 ± 0.07	B18a	1.69 ± 0.24	12.3	6.38 ± 0.9	40	6.9 ± 1.2	16.2 ± 0.3	2.6 ± 0.9
196	2009ig	N	0.84 ± 0.06	B18a	1.64 ± 0.22	22.4	3.37 ± 0.3	10	3.4 ± 0.3	16.3 ± 0.2	1.5 ± 0.4
197	2009le	N	1.02 ± 0.07	B18a	1.40 ± 0.20	16.8	5.31 ± 0.8	25	6.3 ± 1.3	16.2 ± 0.3	2.8 ± 1.1
198	2009Y	N	1.03 ± 0.06	B18a	1.40 ± 0.18	26.3	4.69 ± 0.6	16	5.0 ± 0.7	16.4 ± 0.2	2.8 ± 1.0
199	2010B	N	1.86 ± 0.80	TOSC	0.68 ± 0.39	8.7	1.98 ± 0.5	23	2.0 ± 0.5	16.6 ± 0.3	1.4 ± 0.5
200	2010kg	N	1.36 ± 0.10	TOSC	1.05 ± 0.18	10.7	3.53 ± 0.7	47	4.0 ± 0.9	16.3 ± 0.3	1.9 ± 0.7
201	2011by	N	1.05 ± 0.07	B18a	1.37 ± 0.19	19.9	1.99 ± 0.2	80	7.8 ± 2.3	15.6 ± 0.4	1.3 ± 0.3
202	2011de	03fg	0.75 ± 0.20	TOSC	1.78 ± 0.58	78.2	47.49 ± 3.2	9	47.5 ± 3.3	14.9 ± 0.5	3.5 ± 1.8
203	2011fe	N	1.07 ± 0.06	B18a	1.35 ± 0.18	277.9	9.03 ± 0.2	35	9.2 ± 0.3	15.7 ± 0.2	1.8 ± 0.6
204	2011hb	N	0.99 ± 0.06	TOSC	1.44 ± 0.19	19.4	11.38 ± 1.2	5	11.4 ± 1.2	16.3 ± 0.2	5.7 ± 1.8
205	2011im	N	1.29 ± 0.06	TOSC	1.11 ± 0.15	22.2	7.10 ± 1.6	80	11.4 ± 3.4	16.0 ± 0.5	3.3 ± 1.8

Continued on next page

Table E2 – *Continued from previous page*

ID	SN name	Ia-type	$\Delta m_{15}(B)$ [mag]	ref	$M_{\rm wd}$ [$M_\odot$]	θ ["]	$r_\perp$ [kpc]	ϕ [°]	r [kpc]	$\log_{10}(\rho_\chi)$ [dex($M_\odot$ Mpc^{-3})]	v_χ [100 km s^{-1}]
206	2012cg	N	0.77 ± 0.06	B18a	1.75 ± 0.24	15.0	1.19 ± 0.2	40	2.0 ± 0.6	16.5 ± 0.3	1.1 ± 0.3
207	2012dn	03fg	0.92 ± 0.04	C19	1.53 ± 0.17	36.7	6.94 ± 1.5	65	9.4 ± 2.5	15.5 ± 0.5	1.3 ± 0.5
208	2012fr	N	0.84 ± 0.06	B18a	1.64 ± 0.22	48.1	4.21 ± 0.2	49	6.8 ± 0.9	16.3 ± 0.2	3.4 ± 1.1
209	2012hr	N	1.00 ± 0.06	TOSC	1.43 ± 0.19	93.1	17.93 ± 3.5	76	24.2 ± 6.0	15.2 ± 0.6	2.4 ± 1.4
210	2012ht	N	1.19 ± 0.06	B18a	1.21 ± 0.16	22.1	2.57 ± 0.2	59	4.1 ± 0.6	15.8 ± 0.3	0.9 ± 0.2
211	2012Z	02cx	1.46 ± 0.04	TOSC	0.96 ± 0.13	47.3	7.04 ± 0.6	16	7.1 ± 0.6	15.9 ± 0.2	1.7 ± 0.5
212	2013aa	N	0.72 ± 0.28	TOSC	1.83 ± 0.81	194.6	15.04 ± 7.3	3	15.0 ± 7.3	15.5 ± 0.9	2.1 ± 2.1
213	2013cv	91T	0.87 ± 0.20	TOSC	1.60 ± 0.47	3.3	2.36 ± 1.8	30	2.4 ± 1.9	16.2 ± 0.9	0.9 ± 0.5
214	2013dy	N	0.84 ± 0.06	B18a	1.64 ± 0.22	25.0	2.40 ± 0.2	45	9.0 ± 3.3	15.4 ± 0.5	1.1 ± 0.3
215	2013gs	N	1.16 ± 0.04	TOSC	1.24 ± 0.14	10.7	3.79 ± 0.7	25	5.6 ± 1.8	15.8 ± 0.4	1.2 ± 0.4
216	2013gy	N	1.32 ± 0.06	TOSC	1.09 ± 0.15	33.4	7.04 ± 1.5	4	7.1 ± 1.6	15.7 ± 0.4	1.4 ± 0.5
217	2013Q	N	1.01 ± 0.12	TOSC	1.42 ± 0.27	41.5	14.90 ± 1.8	27	15.5 ± 2.1	16.1 ± 0.2	6.5 ± 2.4
218	2014dg	N	1.07 ± 0.06	TOSC	1.34 ± 0.18	6.2	0.43 ± 0.1	54	0.9 ± 0.4	17.0 ± 0.4	1.1 ± 0.5
219	2015F	N	1.30 ± 0.06	B18a	1.10 ± 0.15	97.3	9.36 ± 0.3	50	10.2 ± 0.6	16.0 ± 0.2	3.2 ± 1.0
220	2016bln	91T	0.87 ± 0.02	C19	1.60 ± 0.14	170.1	82.20 ± 6.2	22	101.0 ± 14.7	14.6 ± 0.5	4.8 ± 2.4
221	2016dwu	03fg	0.67 ± 0.07	C19	1.91 ± 0.30	23.3	6.70 ± 1.1	45	7.4 ± 1.4	15.6 ± 0.4	1.2 ± 0.5
222	2018oh	N	0.96 ± 0.03	L18	1.48 ± 0.15	5.3	1.21 ± 0.4	29	1.3 ± 0.5	16.6 ± 0.3	0.9 ± 0.3
223	LSQ12gdj	91T	0.77 ± 0.04	TOSC	1.75 ± 0.19	27.9	13.40 ± 1.7	17	13.7 ± 1.9	15.1 ± 0.4	1.1 ± 0.3
224	PTF11kx	CSM	1.17 ± 0.06	TOSC	1.23 ± 0.16	6.9	6.35 ± 1.1	14	7.2 ± 1.7	15.8 ± 0.3	1.5 ± 0.4

Table E2: List of SNe used in this work. Ia-types: N = normal, 91bg = SN Ia like 1991bg, 91T = SN Ia like 1991T, 02cx = SN Ia like 2002cx, 02es = SN Ia like 2002es, 03fg = SN Ia like 2003fg, CSM = SN Ia of interaction with circum stellar medium, pec = peculiar SN Ia; $\Delta m_{15}(B)$ = B-band post-peak decline rate over 15 days; references for the decline rate: K17 = Krisciunas et al. (2017), T17 = Taubenberger (2017), B18a = Burns et al. (2018), B18b = Bulla et al. (2018), L18 = Li et al. (2019), C19 = Chen et al. (2019), TOSC = reference in The Open Supernova Catalog (`https://sne.space`); $M_{\rm wd}$ = explosion mass; θ = angular offset (error estimation globally $\delta\theta = 1$"); $r_\perp$ = perpendicular offset from host; ϕ = SN position angle (error estimation globally $\delta\phi = 2°$); r = 3d-offset from host; ρ_χ = local DM density in the vicinity of the SN; v_χ = velocity dispersion in the vicinity of the SN explosion but outside the progenitor WD potential well.

This paper has been typeset from a TEX/LATEX file prepared by the author.